November 2013

Skeletal Muscle Contraction Simulation: A Comparison in Modeling

Jonathan M. Ford
University of South Florida, jford@health.usf.edu

Skeletal Muscle Contraction Simulation: A Comparison in Modeling

by

Jonathan M. Ford

A dissertation submitted in partial fulfillment
of the requirements for the degree of
Doctor of Philosophy
Department of Chemical and Biomedical Engineering
College of Engineering
University of South Florida

Co-Major Professor: Don Hilbelink, Ph.D.
Co-Major Professor: William Lee III, Ph.D.
Susana Lai-Yuen, Ph.D.
Karl Muffly, Ph.D.
Sudeep Sarkar, Ph.D.

Date of Approval:
August 26, 2013

Keywords: Finite Element Analysis, Biomechanics, Kinesiology, Rotator Cuff, Shoulder

DEDICATION

I would like to dedicate this dissertation to my adoptive parents, Gary and Diana Decker of Jacksonville, Florida who have been there for me and cheered me on throughout this whole process. I would also like to dedicate this to my partner in crime, Summer, for always believing in me, especially those times I didn't belief in myself. You've been my best friend and confidant through the majority of my education. I don't doubt you'll be there now that my formal education is done. I am eager to start our next chapter.

ACKNOWLEDGMENTS

TABLE OF CONTENTS

LIST OF TABLES

LIST OF FIGURES

ABSTRACT

Computer generated three-dimensional (3-D) models are being used at increasing rates in the fields of entertainment, education, research, and engineering. One of the aspects of interest includes the behavior and function of the musculoskeletal system. One such tool used by engineers is the finite element method (FEM) to simulate the physics behind muscle mechanics. There are several ways to represent 3-D muscle geometry, namely a bulk, a central line of action and a spline model. The purpose of this study is to examine how these three representations affect the overall outcome of muscle movement. This is examined in a series of phases with Phase I using primitive geometry as a simplistic representation of muscle. Phases II and III add anatomical representations of the shoulder joint with increasing complexity. Two methods of contraction focused on an applied maximal force (Fmax) and prescribed displacement. Further analyses tested the variability of material properties as well as simulated injury scenarios. The results were compared based on displacement, von Mises stress and solve time. As expected, more complex models took longer to solve. It was also supported that applied force is a preferred method of contraction as it allows for antagonistic and synergistic interaction between muscles. The most important result found in these studies was the consistency in the levels of displacement and stress distribution across the three different 3-D representations of muscle. This stability allows for the interchangeability between the three different representations of muscles and will

permit researchers to choose to use either a bulk, central line of action or a spline model. The determination of which 3-D representation to use lies in what physical phenomenon (motion, injury etc.) is being simulated.

CHAPTER 1:

INTRODUCTION

Computer generated three-dimensional (3-D) anatomical models are frequently used in fields such as entertainment, education, research, engineering and a number of other industries. Advances in computed tomography (CT) and magnetic resonance imaging (MRI) have provided opportunities for patient specific 3-D modeling.[1] Computer models of the musculoskeletal system are being increasingly used to study musculoskeletal functions, disorders and potential surgical treatments.[2-9] Utilizing accurate 3-D representations of patient specific anatomy can help provide a scientific basis for studying normal musculoskeletal functionality, disorders and insight on how those disorders may be repaired. Biomedical engineers use computer-aided design (CAD) and the Finite Element Method (FEM) as standard tools in the research, development and performance of orthopedic implants, injury analysis, surgical repair, incident recreation, ergonomic development and a number of other applications.[2-14]

One such area of interest, as applies to human motion studies and orthopedics, focuses on the computer simulated representation of muscle contraction. Studies of this area have utilized a variety of two-dimensional (2-D) and 3-D representations of muscle in conjunction with a mathematical formula representing muscle contraction.[14,15] The 3-D

muscle geometry has been represented as a lump or bulk model, a cylinder representing a central line of action (or a small number working in conjunction) or a series of splines representing the general direction of muscle fibers.[7,8,16-18]

Mathematically, muscle contraction is represented as variations of either the Hill's muscle model[19] or Huxley's model[20] of muscle contraction. Both the Hill and Huxley mathematical models are solving the same physiological process but use either a more phenomenological or a more biochemical/biophysical approach, respectively. Most of the current movement analysis software and recently published papers utilize the Hill model. The Huxley model is almost exclusively utilized by biophysicist and biochemists to understand the mechanisms of contraction at a molecular level. Huxley's model is considered "elegant" but too complicated to serve directly as a mathematical representation of muscle contraction in motor control studies. Hill's mathematical model is used almost as equally as exclusively by bioengineers and movement scientists.[21] The goal of this study is to develop a methodology comparing the three different representation of 3-D muscle geometry utilizing Hill's mathematical model that is both accurate and time effective within a commercially available Finite Element software package.

Anatomy

Skeletal muscles are the contractile centers of human motion. They are connected to bones via tendons or aponeuroses at their respective origins and insertions. Certain

muscles may have more than one origin or insertion. When muscles contract, the fibers that make them up shorten to roughly 70% of their resting length. During contraction the muscle's origin usually remains fixed while the resulting movement occurs at the insertion. There are three methods of skeletal contraction. One is reflexive, which as the name implies, is not voluntarily controlled. Tonic contraction is a slight contraction that basically give muscles their firmness or tone. The third type of contraction is phasic contraction which in turn consists of isometric contraction and isotonic contraction. Isometric contraction increases the muscle tension, but no muscle shortening occurs. Isotonic contraction results in changes to the muscle length.[21-24]

Tendons are the dense fibrous tissues that connect muscles to bones. Collagen Type I makes up roughly 70-80% of a tendon's dry weight. Tendons vary in size and shape based on the attachment points for each muscle. They can be narrow chord-like structures or broad and sheet-like. Typically, tendons consist of the outer "tendon" structure and the internal structure, called the aponeurosis. The "tendon" portion provides attachment to bone, while the aponeurosis area provides anchorage to the muscle fibers. The primary role of a tendon is to transmit the generated muscle forces to the bone. Since muscles can only pull and not push, tendons need to be stiff and strong under tension. It is this strong and stiff characteristic of tendons that prevent them from substantially being deformed during loading.[21-24]

The structural unit of the muscle is the muscle fiber. Muscle fibers usually have a diameter of 10-60 µm. Fiber length can vary, depending on the length of the muscle and

whether or not the fiber extends only for a part or the entirety of the muscle. These fibers are made up of myofibrils which in turn consist of myofilament bundles. These myofilaments are divided transversely by the zwichenscheibe (Z) bands which are the demarcation line for sarcomeres. Each sarcomere is roughly 2.5 µm long. Two types of myofilaments are present in the sarcomeres. The thinner (5 nm diameter) actin molecules and the thicker (12 nm) myosin molecules act in conjunction to produce muscle forces. The actin filaments make up the anisotropic (A) bands in skeletal muscle while the myosin filaments make up the isotropic (I) bands. A globular head on the myosin filaments acts as a "ratchet" that creates a cross-bridge to the neighboring actin filaments. As a result, the two filaments slide parallel to one another and generate the muscular force. It should be noted that the resultant muscle contraction is not generated by a contraction of the filaments themselves but rather the sliding of the actin and myosin filaments. The lengths of the actin and myosin filaments are not altered during muscular contraction.[21-24]

The gross anatomy that this study will focus on consists of the human shoulder joint and the skeletal muscles that make up the rotator cuff. The shoulder joint consists of the humeral head and where is articulates with the scapula, namely the glenoid cavity. The glenoid cavity is relatively shallow and is slightly deepened by the cartilage making up the glenoid labrum. The humeral head is held in place by the four muscles of the rotator cuff. These four muscles are the supraspinatus, infraspinatus, teres minor and the subscapularis. Each of these muscles has their origin in the scapula and insert into the lateral/superior aspect of the humeral head. A loose fibrous capsule surrounds the

4

glenohumeral joint. It attaches along the margin of the glenoid cavity and the anatomical neck of the humerus.[25]

Clinically, the rotator cuff is a common injury of the upper limb. Activities that bring the upper limb above the horizontal plane (such as throwing, tennis, swimming, or weight lifting to name a few) present a higher risk of rotator cuff injury. Repeated motions of the upper limb can cause the humeral head and rotator cuff to impinge on the coracoacromial arch which can cause inflammation of the rotator cuff as a whole. This inflammation can have a degenerative effect on the supraspinatus and may cause a complete tearing of the muscle. As a result the supraspinatus will be no longer functional and initiation of abduction of the upper limb is no longer possible.[25]

Visible Human Project

The field of biomedical engineering applies the principles of engineering to a biological setting. Technological advances in the past few decades have made it possible to perform CAD and FEA on biological structures. These advances have opened up new avenues for biomedical engineering research and development. With a push toward patient specific medical procedures, speed and accuracy in the development of 3-D anatomical models are important.[26,27] Medical imaging is one of the primary tools used in surgical planning and sources for engineering research. However, each imaging modality has its limitations. CT scanning works best when focusing on bones, contrast agents or larger structures. The finer structures such as ligaments and joint capsules

can be difficult to visualize using CT scans. MRI scans are better at imaging soft tissues, but often fail to have clean edges which present segmentation issues and require a sound anatomical knowledge to do so.

One of the first datasets created that addresses some of the limitations of medical image modalities is the National Library of Medicine's *Visible Human Project*. The initiative was undertaken with the goal to create a digital volumetric collection of complete normal adult male and female anatomy. The Visual Human Male (VHM) dataset was completed in August of 1993. The specimen was that of a 39-year-old male incarcerated on death row in the Texas prison system and who had donated his body to science. The man's body was frozen and serially milled over a period of 128 days in a custom cryomacrotome developed by the University of Colorado. A series of film and digital photographs were taken for each 1 mm slice through the specimen.[28]

The VHM dataset images are comparable to modern CT and MRI scans with a slice thickness of 1mm and a pixel size of 0.353 x 0.353 mm. In addition, this dataset has the added benefit of color which aids in the segmentation process by being able to cleanly distinguish between structures such as tendon and ligaments. The 1,878 axial images are tiff files that are 1760 x 1024 pixels in size with a resolution of 72 dpi and in total take up roughly 9.5 gigabytes of space. The dataset is public domain and available from the National Library of Medicine (NLM).[26] Following release of the VHM, a number of similar projects were undertaken. In the years that followed, the NLM released the

Visible Human Female. Other groups released their own versions such as the Visible Korean Project and the Visible Chinese Project.[29,30]

What makes the Visible Human datasets unique is the ability to observe the anatomy of an entire individual in situ. The spacing of organs and structures remain in their natural location as they were in a living body. For the first time, the availability of these high-resolution images provided the opportunity for the accurate reconstruction of the human body. High-resolution anatomically accurate 3-D models of the Visible Human Male and the Visible Chinese projects have been visualized and manipulated using readily available software and analyzed and measured using application based software for CAD and FEA.[16, 31]

Finite Element Analysis

The Finite Element Method (FEM) or Finite Element Analysis (FEA) has become standard practice in the development of models and simulations for a variety of engineering projects. The term was first coined by R.W.Clough in 1960 with his discussion concerning plane stress analysis.[32] The lessons learned from the early applications of FEA were quickly adopted and utilized the fields of thermal, fluid flow and piezoelectric process. FEM is now used in transportation, electrical, communications, housing, environmental, acoustical, as well as biological and medical applications. The ability to model, visualize, analyze, simulate, prototype and fabricate

structures has opened up the possibilities and the usefulness of computers in the engineering process.[32-35]

The main goal of FEM is to determine the distribution of a property throughout the structure based on a set of partial differential equations. A few common examples of these potential properties can be temperature disbursement, the displacement from an applied stress, or the distribution of an electrical charge. At the beginning of this process, it is up to the engineer to calculate how the acting agent is applied to the geometry. This agent can take the form of force, electrical current, temperature and so on. The result is an approximated solution that numerically represents the distribution of a problem that would be considerably difficult to obtain manually. FEM can be applied to one-dimensional, two-dimensional, three-dimensional and four-dimensional problems. For 3-D geometries, the model is sectioned into a number of simplistic geometric elements. These elements range from tetrahedral (four-sided), brick (8-sided) to hexahedral (6-sided) in shape. The number of elements is finite and in turn each element has a set of known physical laws and finite parameters applied to it. The process creates a set of linear algebraic equations that are run simultaneously to solve the system.[33,.35]

The real objects and their relative components can be rather complex and often need to be decimated so that the finite element software package can handle the geometry. The structure's geometry is created from the collection of elements that provide a discretized approximation of the object's curves in a piecewise fashion. This occurs via a process

known as "meshing". The accuracy of a curve's representation hinges on the number of elements that are used in the mesh. It follows that the closest representation of a structure would have the highest number of elements. However, each element requires its own computation. Due to software and hardware limitations, it is essential to cap the number of elements used. On account of these limitations, the finer details of a structure are often omitted. It is up to the designer or modeler to determine whether or not the smaller details are critical to the overall structure. Exclusion is considered acceptable, if these details play only an aesthetic or minimal role in a model's performance. The results of the analysis need to be observed with these omissions firmly in mind. In the end, all finite element analysis results in the approximation of the structure or structures being studied. It may be a very close approximation, but it is still an approximation nonetheless.[34]

The creation of a mesh can be an arduous process. The length of time needed in mesh creation lies in the object's complexity and the experience of the analyst. Meshing via triangulation is the most common form of element creation. Unlike brick meshes, the creation of tetrahedral meshes is highly automated in most pre-processing software. Tetrahedral meshes also have the added advantage of being able to tackle complex organic geometries. However, the speed and ease of tetrahedral meshes comes at the cost of accuracy. Brick element meshes are considered more accurate, but their lack of automation decreases their use.[34]

Once the mesh is created the object is assigned material properties. Objects can be made up of multiple materials based on the Young's modulus and shear modulus of the desired material. These properties can be assigned to a group of elements or to each individual element. Commercially available FEM packages often come with a built-in library of known material values. These usually consist of different types of metals and other materials such as wood or glass. Most packages do not come with biological materials and the properties for these items need to be furnished from experimental data. A number of publications exist that have suggested material properties for objects of a biological origin, such as bone or soft tissue.[34-38] The solving of the computational model utilizes a computer's Central Processing Unit (CPU) and the Random Access Memory (RAM). Obviously, the functionality of a computer improves as its processor and memory power increases.

There are a number of Finite Element (FE) software packages available for commercial use. A few of note include *COMSOL*[41], *ANSYS*[42] and *Abaqus*.[43] Each package is designed to accept a variety of file formats. Templates for common applications, such as electrical, thermal, acoustical, structural, fluids scenarios, are usually provided. All of these packages allow for user customization so the analyst has full control of their model and simulation. As multi-physics packages, it is possible to include more than one physics interaction. For example, a finite element analysis can be run on a circuit for multiple scenarios. One analysis can compute the flow of electricity, while another determines the heat that corresponds with the generated electric current. Structure

geometry can be created using native creation tools or imported from another software package.

Human Applications

In practice, FEA can be used as a precursory step to predict the outcome of a physical event before actually running an experiment or manufacturing an expensive prototype. Applying FEM to the study of human anatomy permits detailed analyses of complex virtual anatomical models under simulated experimental conditions. Despite the current level of today's computer technology, there are still limitations to applying FEA for biological models. The complex geometries and the subtle details of anatomical structures can prove too intricate for FEA to work. As a result, 3-D models must often be simplified to such an extent that a significant reduction in anatomical detail may result. It is unclear as to how much simplification can occur before the simulation no longer represents a real life scenario. More recently, studies have been conducted on what role mesh density plays in biological and anatomical scenarios. Recent studies by the author suggest that mesh density can be dramatically reduced without drastically affecting FEA results.[44] However, others have concluded the opposite and stated that predicted results depended heavily on mesh density.[3] The importance the role mesh density plays in finite element analysis may lie in what manner of physical activity is being simulated.

FEA has been applied to humans and has assisted in a variety of medical and design fields.[45] The mechanical behavior of the femur using a 2-D model was analyzed as early as 1972.[4] Blood flow[10], arterial wall pressure[11], foot tread analysis[6], orthopedic implant design and testing[5], traumatic brain injury analysis[13] and a number of other medically applicable studies have utilized the tools of the finite element method. Medical implant design and performance have also benefitted from finite element simulations.[7] Furthermore, the FE method has been applied to human models for design purposed in the automobile industry. One such example involves the creation of a model of the human body for restraint system testing applications.[12]

Of all the representations of biological tissues, the representation of bone is fairly standard in most computer models. Bones are treated as rather stable elements that react to muscle movements. It is the representation of muscle, on the other hand, that has variety of both very simple and very complex ways in how it is modeled in computer simulations.

There are three main ways of representing muscles in 3-D. The first type looks at a "lump" model to capture the muscles' bulk shape.[16] Another type of muscle model consists of one or more cylinders or tubes to represent the muscle geometry. Very often this type of muscle has at least one central tube representing the muscle's central line of action (CLOA).[7,8] Software, such as *Software for Interactive Musculoskeletal Modeling* (*SIMM*),[46] *LifeModeler*,[47] and *AnyBody*[48] have been developed to simulate the biomechanics of movement in both humans and animals. These software packages

often utilize segments to control the model's movement.[49] The CLOA may be accompanied by additional cylinders or segments to represent a particularly broad muscle origin or subdivisions within a muscle. There have been attempts to model the complex 3-D muscular geometry by focusing on the fibers that make up the muscles themselves. Some studies focus on the perpendicular arraignment of muscle fibers to try and capture shear stress and analyze stretch distributions during muscle exertion.[50] Still others try capture the 3-D arrangement and lengths of the muscle fibers to capture muscle behavior.[17] These studies all focus on the 3-D geometry of the muscle to varying degrees of complexity.

Mathematical Models for Muscle Contraction

Biological soft tissues tend to have highly nonlinear mechanical behavior with associated passive elements that can either be described as nonlinear hyperplastic or viscoelastic. Skeletal muscles have the added complexity in that they can generate tension forces resulting in the contraction and relaxation of their geometry. There are two current mathematical models for muscle contraction, namely the Hill's model[19] and the Huxley or Sliding Filament Theory of Muscle Contraction.[20] The Hill's model for muscle contraction is being used as the basis for the commercial human modeling systems such as *LifeModeler* and *AnyBody.* The Hill's model is chiefly used by bioengineers and movement scientists. Huxley's model takes a more biochemical approach to muscle contraction by looking at displacement of muscle cross-bridges as the actin and myosin fibers slide across one another. Both mathematical models can be

entered into standard FE software packages. Both the Hill and Huxley mathematical models are solving the same physiological process but use either a more phenomenological or more mechanistic approach, respectively. Most of the current movement analysis software and recently published papers utilize the Hill model most likely on account of its relatively straight forward and simplified approach as compared to the Huxley method. For the purposes of this study, Hill's model of muscle contraction will be used.[21,22]

The Hill's Equation for Tetanized Muscle contraction was developed by Archibald Hill from his observations of frog sartorius muscle contractions. The initial equation is

$$(v + b) + (P + a) = b(P_0 + a)$$

where P represents tension in a muscle, v represents the velocity of contraction and a, b and P_0 are constants. Hill discovered that there is a hyperbolic relation between P and v. A higher load will have a slower contraction velocity. The higher the velocity, the lower the tension. This relation was in direct contrast to the viscoelastic behavior of passive materials and it was shown that the active contraction of a muscle had no resemblance to the viscoelasticity of a passive material. However, the original Hill equation only focused on the quick-release of a muscle in tetanized conditions, and did not account for single twitch, slow muscle release or strain as it varies with time.[21, 22, 24]

Expanding on the original model, Hill's Three-Element Model was developed. This model represents an active muscle composed of a 1) contractile element (CE), 2) a series element (SE) which is arranged in a series with the contractile element and 3) a

parallel element (PE) which accounts for the elasticity of a muscle at rest. A schematic can be seen in Figure 1.1.
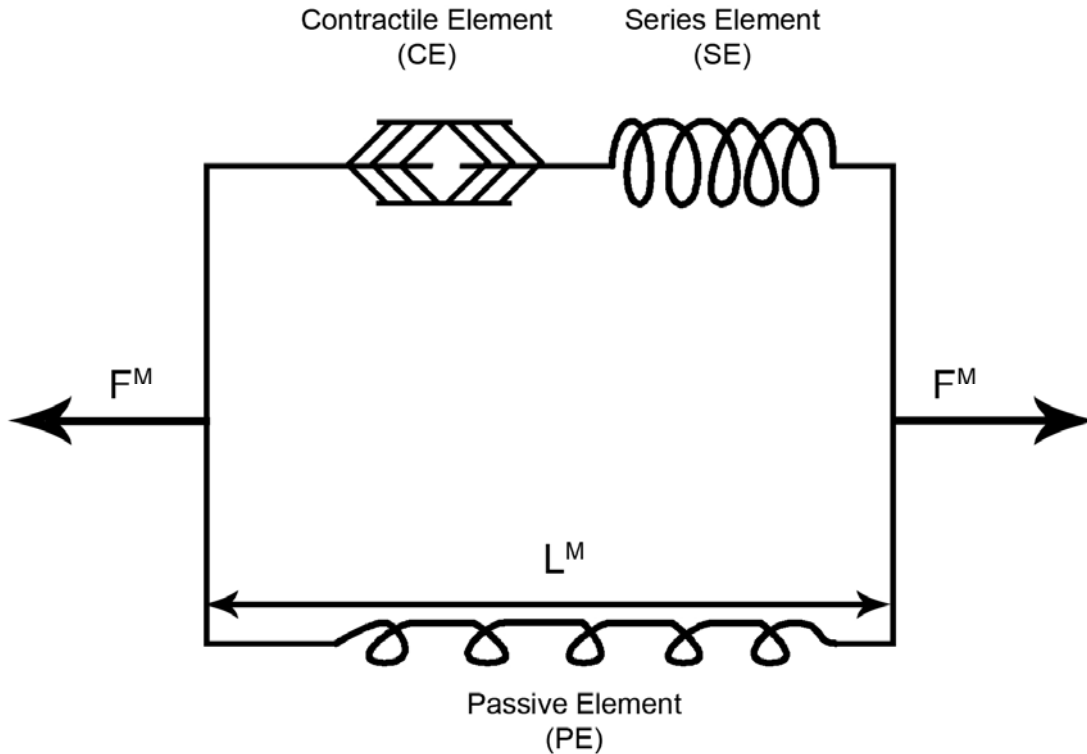
Figure 1.1: Hill's Three Element model

The CE is freely extendable when inactivated, but capable of shortening when activated. The SE is a nonlinear spring arranged in series with the CE and allows for rapid change in muscle from inactive to active. The PE is another nonlinear spring arranged in parallel to the CE and SE elements, and is responsible for the passive behavior of the muscle. The active force of the CE is generated by the myosin and actin cross-bridges of the muscle. The net force relationship to muscle length is the combination of the force-length of the passive and active elements of the model represented by $F = F_{PE} + F_{SE}$ and $F_{CE} = F_{SE}$. The muscle length is represented as $L =$

L_{PE} and $L = L_{CE} + L_{SE}$. L_0^M represents the rest length of the muscle. When it is fully activated, it creates the peak isometric muscle force, F_0^M. When inactive the $F_{CE} = F_{SE} = 0$ and the muscle has a force in the PE. When activated, the resulting muscle force of the CE depends on the muscle length and the velocity of the CE's deformation.[51]

The maximal force (F_0^M) can be calculated by using either the physiological cross sectional area (PCSA) or the anatomical cross sectional area (ACSA). The ACSA takes a cross section and calculates the area through a plane central to the belly of the muscle. The PCSA creates a multi-faceted plane perpendicular to the flow of muscle fibers. For bi-pennate or multipennate muscles, this "plane" may be a multifaceted zigzag through the muscle. The equation is calculated as: $PCSA = \frac{muscle\ volume}{fiber\ length} = \frac{muscle\ mass}{density\ \cdot\ fiber\ length}$. The total force is calculated as Total force = PCSA·Specific Tension. For pennate muscles, the Muscle force = Total force·cosθ, where θ is the angle of the muscle fibers. For muscles where all the fibers run parallel the PCSA = ACSA. Another aspect on importance in determining muscle force is the relative mixture of fast and slow twitch fibers within the muscle. This combination of fast and slow twitch fibers has a direct effect on the muscles relative maximum velocity of contraction.[52, 53]

Study Organization

The study was conducted in a series of three phases. Each phase increased the level of complexity. The level of displacement, von Mises stress, model complexity and solve

time were all recorded and compared across the bulk, central line of action and spline scenarios for each phase.

Phase I

Phase I began with a pilot study examining a very simple geometry as a representative for anatomical structures. This was done with a basic geometry of two cubes (representing bone) connected by one central bar (representing the muscle) with representative tendons. This central muscle was represented as a lump model, a central cylinder model and a series of splines. Each representation of the muscle then contracted utilizing the Hill mathematical formula. The same amount of force was applied in each case. The resulting stresses and the overall displacement was compared to see if there was any statistical difference between the three different representations of muscle contraction. The total time for each scenario, from model construction through the analysis was recorded to test for time efficiency. Figure 1.2 contains the Phase I lump, central line of action and spline geometries respectively.

Phase II

Phase II consists of a similar methodology, with the simple geometry being replaced by an anatomical model derived from the VHM dataset. Two bones, consisting of the left scapula and left humerus were created with one of the muscles of the rotator cuff, the teres minor, connecting the two. A representative joint capsule was created to hold the

joint in place during movement. The teres minor was represented as a bulk muscle, a series of splines, as well as a tube running from the centroid of the origin, through the central axis of the muscle and to the insertion. Each scenario was run using the Hill mathematical representation of contraction. The same amount of force was applied in
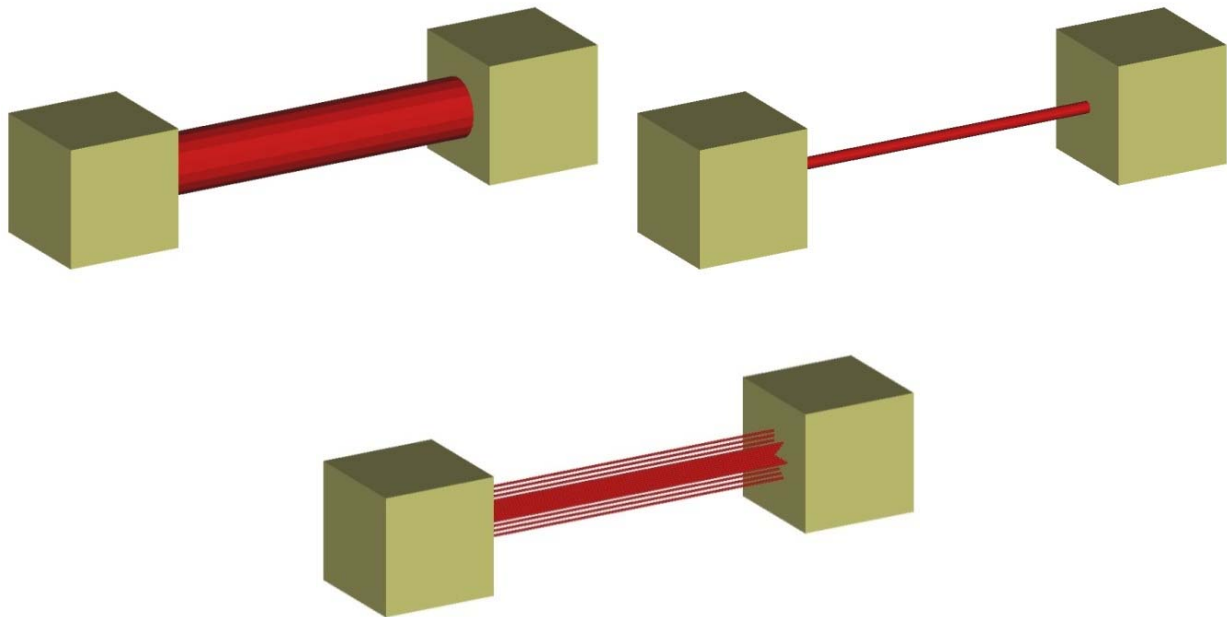
Figure 1.2: Phase I representations of the lump, central line of action and spline muscle geometries

each case. The displacement of most distal point of the humerus was compared for the three different scenarios. The total time for each scenario, from model construction through the analysis was recorded to test for time efficiency. Figure 1.3 contains representations of lump, central line of action and spline geometries for Phase II.

Phase III

Phase III expanded on Phase II with an increasingly more complex shoulder model. The muscles of the rotator cuff (the supraspinatus, the teres minor, the infraspinatus and the subscapularis) were represented. The shoulder muscles contracted to make a series of standard physical motions, such as abduction or forward shoulder flexion. The displacement of most distal point of the humerus was compared for the three different scenarios. The total time for each scenario, from model construction through the analysis was recorded to test for time efficiency.
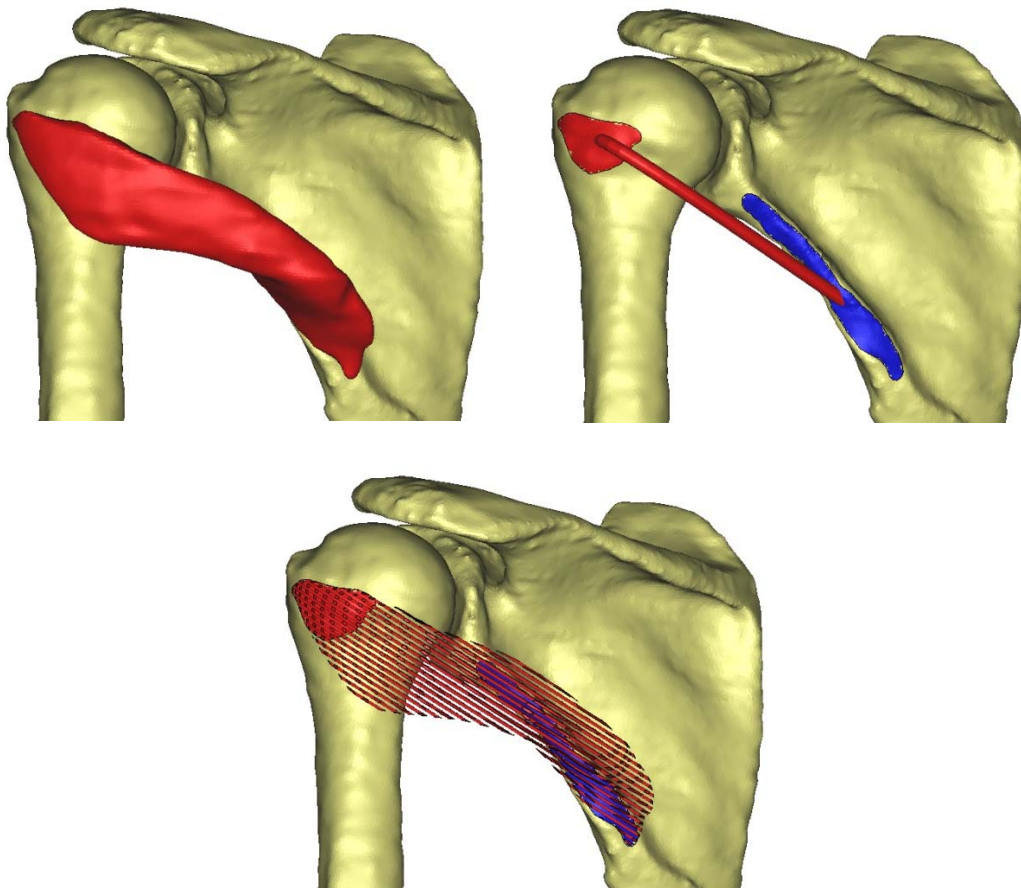
Figure 1.3: Phase II representations of the lump, central line of action and spline muscle geometries.

To accomplish the three phases of the project, the number of specific aims are proposed:

1. Create the 3-D geometry representing bone and muscle.

2. Import and run the created geometry into a standard finite element software package where the Hill mathematical model is used.

3. Determine what effects the different representations of 3-D muscle geometry in combination with linear material properties and maximal muscle contraction have on resulting stresses and displacement.

Conclusion

Technological advancements in computers, simulation and medical imaging have opened new avenues for musculoskeletal biomechanical research. The creation of anatomically accurate human models is now possible and CAD and FEA studies using these models are gaining in popularity. The time needed for the creation of anatomical models and the development of the muscle models all hinge on the complexity of the geometric representation. The more complex a finite element model is, the longer it takes to create. With the medical industry's push for more patient specific implants and medical procedures, total case turnaround time is essential. However, researchers must be careful that they do not sacrifice accuracy in the process. One of the key features of FEA is that it is a simplified approximation of a real physical occurrence. The question remains as to how much simplification can occur before it affects the performance of a model.

The purpose of this project was to examine how different levels of simplification and representation of muscle geometry can affect the performance of a finite element anatomical model. This was examined by utilizing three different geometric muscle representations in conjunction with the Hill mathematical model. Model creation time, FEA solve time and results for the three different scenarios were compared.

CHAPTER 2:

PHASE I: SIMPLE GEOMETRY

Abstract

Phase I is a pilot study examining a muscle contraction simulated in a commercially available finite element analysis (FEA) software package using very simple geometry as a stand-in for anatomical structures. This was done with a basic geometry of two cubes (representing bone) connected by one central bar (representing the muscle) with representative tendons. This central muscle was represented as a lump model, a central cylinder model and a series of splines. Each representation of the muscle then contracted by using the physiological cross-sectional area to determine the maximum Force in agreement with the Hill mathematical formula. The same amount of force was applied in each case. The resulting von Mises stresses and the overall displacement were compared to see if there is any statistical difference between the three different representations of muscle contraction. The total time for each scenario is recorded to test for time efficiency.

Introduction

Skeletal muscle is one of the major areas of interest in the study biomechanics and human motion studies. Skeletal muscles have the ability to generate their own force and do not rely on external forces to create strain and deformation. Several muscle models exist that attempt to describe the mechanical behaviors of skeletal muscle. These muscle models are built around either the Hill or Huxley mathematical models for muscle contraction.[19,20] The Hill model is what is predominantly in biomechanical studies.[21] Research on the modeling of force-length relationships, force-velocity relationships and physiological (or anatomical) cross-sectional area has provided mathematical tools to assist the simulation of skeletal muscle contraction.[21, 22, 52-58]

The mathematical representation of skeletal muscle, has been used in conjunction with a variety of two-dimensional (2-D) and three-dimensional (3-D) representations of muscle geometries. 3-D muscle geometry has been represented as a lump or bulk model, a cylinder representing a central line of action (CLOA) (or a small number working in conjunction) or a series of splines representing the direction of muscle fibers.[21, 57-59]

In an effort to test the different 3-D representations of skeletal muscle, this study was undertaken to directly compare the bulk, CLOA and spline muscle geometries. This study examined a very simple geometry as a stand-in for anatomical structures. This is done with a basic geometry of two cubes (representing bone) connected by one central

bar (representing the muscle) with representative tendons. This central muscle is represented as a lump model, a central cylinder model and a series of splines. Each representation of the muscle contracted Hill mathematical formula utilizing the physiological cross-sectional area (PCSA) to calculate the maximum force (Fmax). The same amount of force was applied in each case. The resulting stresses and the overall displacement was compared to see if there was any statistical difference between the three different representations of muscle contraction. The total solve time for each scenario was recorded to test for time efficiency.

Materials and Methods

Models

The 3-D geometry was created within *3-matics* by Materialise. It was decided to use a design pipeline that utilized the import methods of the various software used in this study. The geometries used in Phase II and Phase III required that the anatomical geometry be made within the *Mimics* software package. The FEA package *COMSOL* does have the ability to great primitive based geometries natively, but the anatomical models from Phase II and Phase III will require the meshing and export capabilities of *3-matic*. The decision to use *3-matic* as the initial modeling method for Phase I was made so the meshing treatment for the geometries used in each phase would be uniform.

The three geometries used in Phase I had the same basic structure. Two cubes with the dimensions of 10 cm x 10 cm x 10 cm represented bone. A central geometry represented the muscle-tendon complex with a total length of 25 cm. The muscle was 20 cm in length with the tendons at either end measuring 2.5 cm long. Geometries representing a bulk, central line of action and a series of splines were created. The bulk geometry muscle and tendon all had a radius of 2.5 cm. The muscle was subdivided into five segments each with a 4 cm length. The CLOA had a radius of 0.5 cm with a similar subdivision of five 4 cm segments. The spline model consisted of 33 splines with a 1 mm radius each. Each spline was also subdivided into five 4 cm segments. A representative image of the bulk, CLOA and spline geometries can be seen in Figure 2.1.

After the geometries were created, each structure was connected as a non-manifold mesh. Once the initial step of the modeling was complete, each model was subjected analysis, quality control and remeshing. In this program the 3-D geometry was cleaned up and converted to a volumetric mesh. The initial model clean up began with a Triangle Reduction filter which had a flip threshold angle of 15° and a geometrical error of 0.05 mm. Model cleanup continued by applying a smoothing factor of 0.7 to the object. Surface subdivisions on the mesh were assigned at this step to ensure at a standardized shape and location was maintained through the process. Once these steps were complete, the model was then inspected for any intersecting or overlapping triangles. Any errors in mesh quality were fixed. Each model then underwent a series of processing steps involving: auto-remeshing and quality reduction of triangles of the

geometry. The overall model was inspected a final time for intersecting or overlapping triangles and then converted into a volumetric mesh.

Calculations

For Phase I, muscle contraction was simulated for Fmax generation. Thereby the muscle was at its' highest level of contraction and the contraction velocity was zero. Fmax was calculated using the PCSA * Muscle Specific Tension. The muscle specific tension (or muscle stress constant) was assumed to be 330 kPa.[21] PCSA is calculated as the volume of the muscle divided by the optimal fiber length. This experimental muscle was treated as a parallel muscle. For that reason a muscle length to optimal muscle fiber ratio of 0.9 was used.[16] The optimal fiber length was determined to be 18 cm. PCSA was the calculated as the volume of the muscle (392.7 cm^3) divided by the fiber length (18 cm) for a PCSA of (21.82 cm^2). Fmax resulted in 720 N (21.82 cm^2 * 33 N/cm^2). The data was entered into the Hill equation $(v + b) + (F + a) = b(F_{max} + a)$ and resulted in the stereotypical force-velocity and power-velocity curves.[19,21,23]

COMSOL

A 3-D solid Structure mechanics module was used for the muscle contraction. A step function was used as the basis for the applied force. The idea was to capture the muscle at its most contracted state (velocity = 0 at F=Fmax). Upon the completion of the geometric modeling, the surface and volume meshes were then exported as MPHTXT
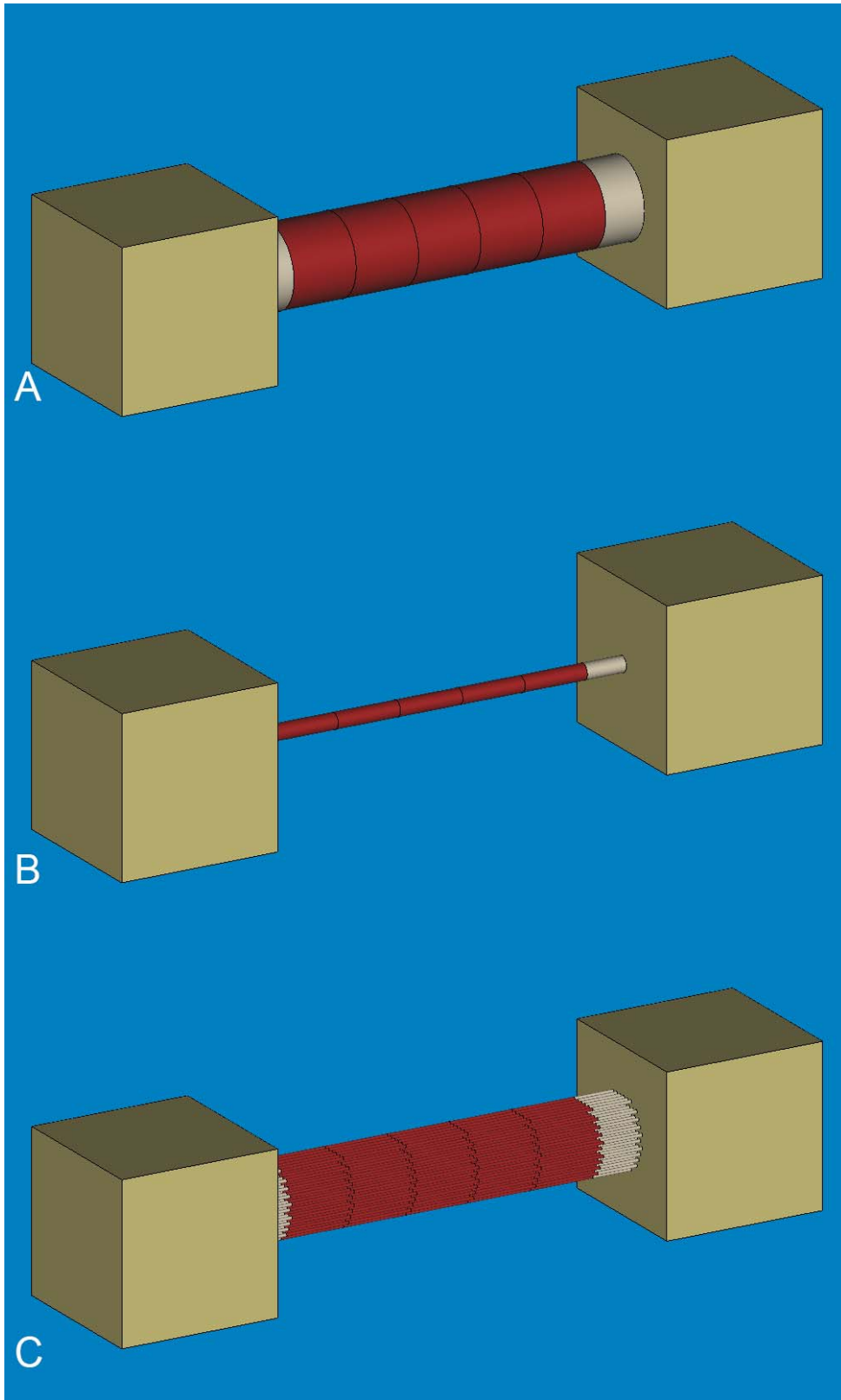
Figure 2.1: Representative lump (A), central line of action (B) and spline (C) geometries.

files, the *COMSOL* ready mesh format. With the mesh imported, material properties were assigned to the relative geometries.

The representative bones were given a Young's modulus of 1.0×10^{10} Pa, a Poisson's ratio of 0.3 and a density of 2570 kg/m^3.[60] The representative muscle was given a Young's modulus of 1.162×10^6 Pa, a Poisson's ratio of 0.4 and a density of 1056 kg/m^3.[60] The tendon was given a Young's modulus of 1.6×10^6 Pa, a Poisson's ratio of 0.497 and a density of 1670 kg/m^3.[61] The left most face of the left bone block was constrained. Boundary loads were applied as force per unit area. Since PCSA was used instead of ACSA, the applied force of 36.67 N/cm^2 was applied in the x and –x axes. The boundary loads were applied to the face of each segment. The forces were only applied along the x axis as the muscle did not deviate in the y or z axis. The model was then solved and displacement and von Mises stress were collected. Solution time data was also collected. This was done for the bulk, CLOA and spline models. FEA analysis with *COMSOL* was run on a Dell Precision T7500 with an Intel Xeon CP X5690 @ 3.47 GHz and 96 GB of RAM.

Results

Three different representations of a stylized muscle were created. The different representations consisted of a bulk, CLOA, and spline constructions. The meshes for each representation had 126,704, 75,023 and 2,243,129 tetrahedral elements respectively. The solve time in *COMSOL* for each scenario was 64 seconds, 69

seconds and 930 seconds respectively. Displacement was captured from the far face of the right block. This represented the greatest amount of displacement on each scenario. Von Mises stress was also captured from the data. Measures of central tendency and a 95% confidence interval were calculated. The element count, solve time, displacement and von Mises stress can be seen in Table 2.1. A visual representation of the displacement can be seen in Figure 2.2. A visual representation of von Mises stress distribution can be seen in in Figure 2.3.

Table 2.1: Phase 1 Data

Scenario	Element Count	Solve Time	Displacement	von Mises Stress
Bulk	126,704	64 s	63.25 mm	39.91 N/cm^2
CLOA	75,023	69 s	63.75 mm	40.4 N/cm^2
Spline	2,243,129	930 s	63.48 mm	41.4 N/cm^2
Average	-	-	63.49 mm	40.57 N/cm^2
St. Dev.	-	-	0.25 mm	0.76 N/cm^2
95% Conf. Inter.	-	-	63.21 - 63.77mm	39.71 – 41.43 N/cm^2

Discussion and Conclusions

The data concerning element count and solve time was not surprising. As a rule with FEA, a higher the number of elements corresponds to a longer solve time. However, even with the most complex geometry of the spline model, the time needed to solve the analysis was relatively short. These solve times are anticipated to increase in Phases II and III as the model complexity increases.
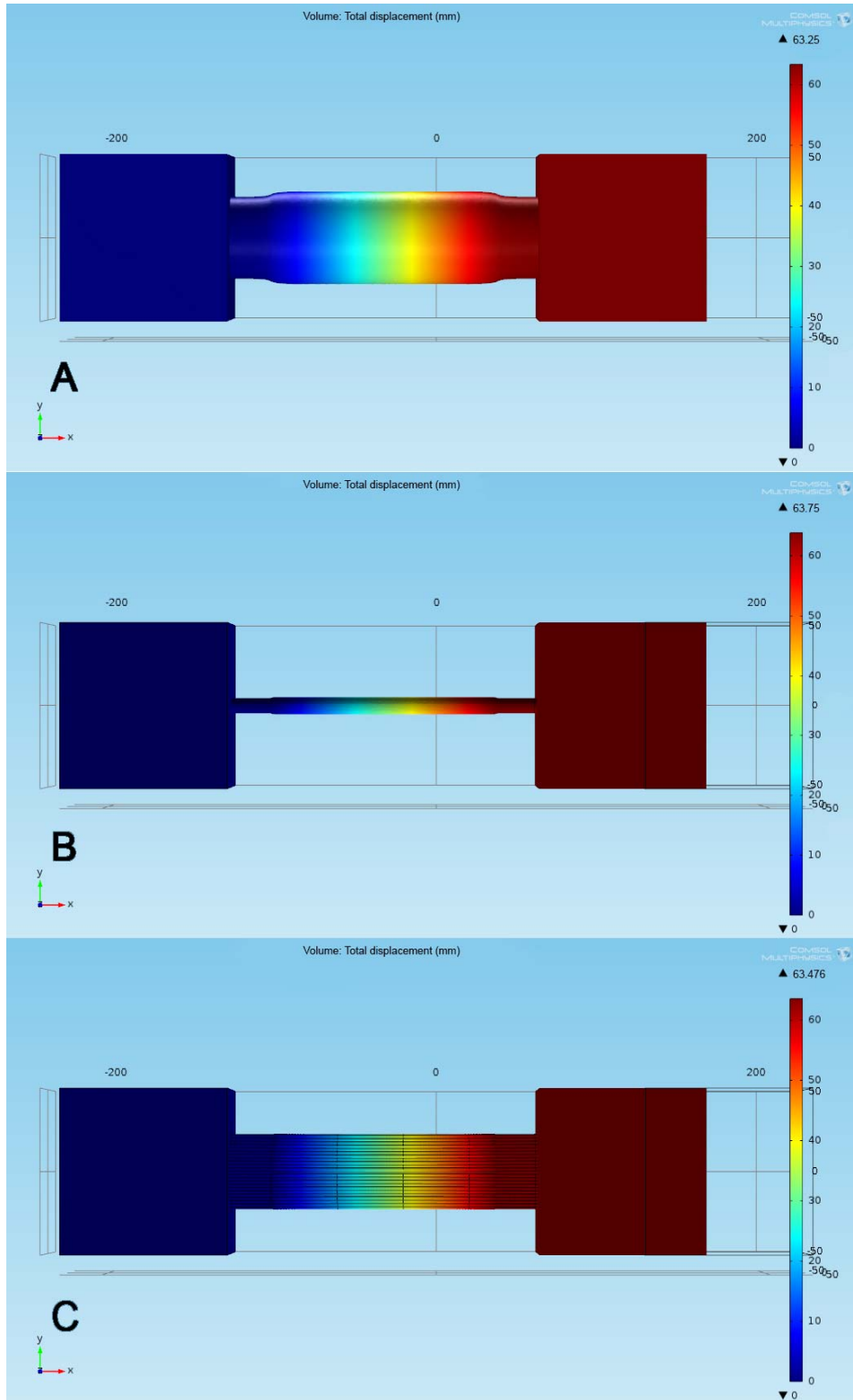
Figure 2.2: Displacement for lump (A), central line of action (B) and spline (C) geometries.
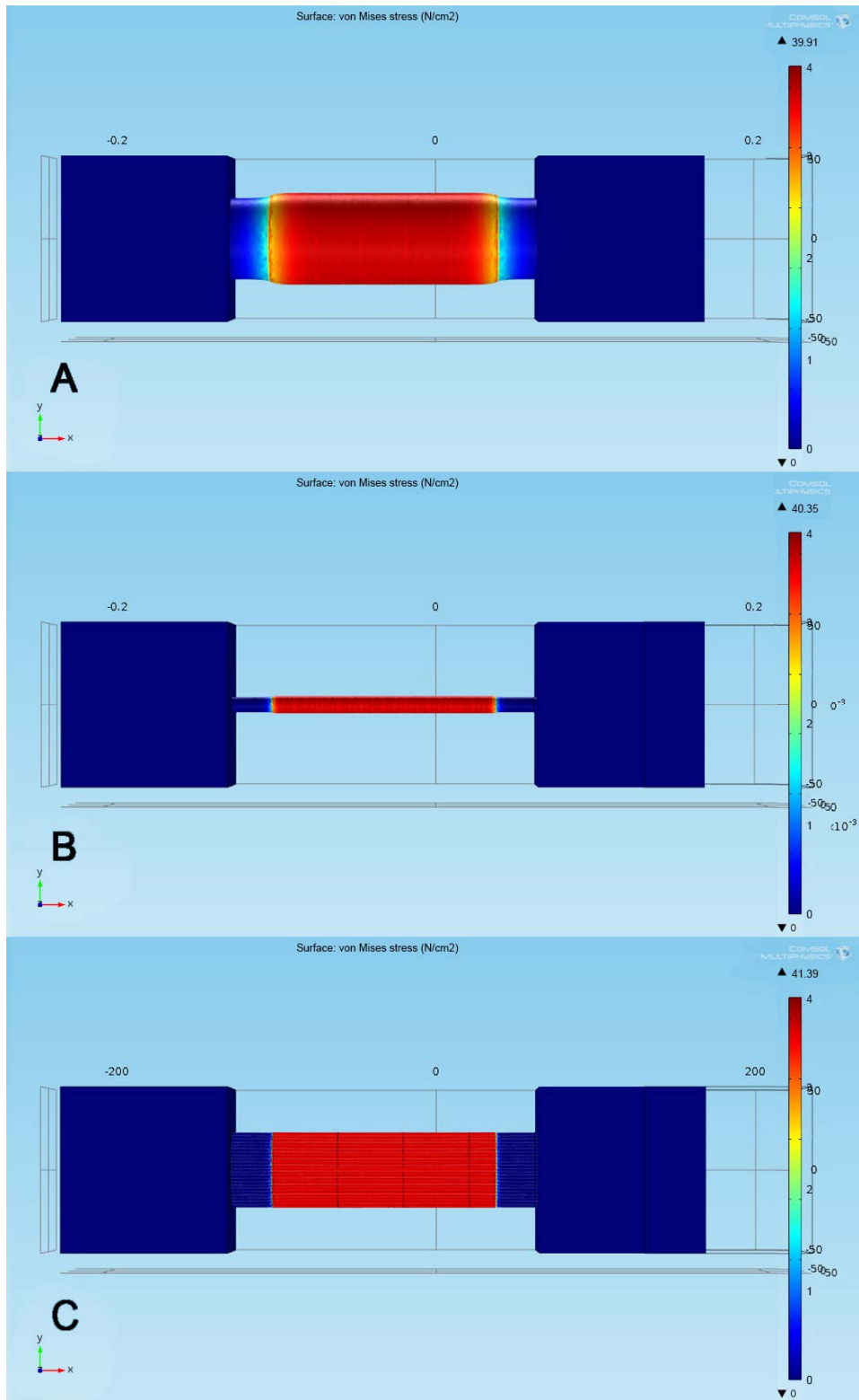
Figure 2.3: von Mises stress distribution for lump (A), central line of action (B) and spline (C) geometries.

An average displacement 63.49 mm with a 95% confidence interval of 63.21 mm - 63.77 mm falls within the range of the 60 mm – 70mm expected from the maximum contraction of a 200 mm muscle.[62] For each scenario, the von Mises stress displayed that the tendon acted as a damper in force transmission from muscle to bone as anticipated.[63,64] The von Mises stress appears relatively stable as well with a 95% confidence interval of 39.71 N/cm^2 – 41.43 N/cm^2 but there does appear to be an upward trend as the diameters of the muscle geometries narrow. This trend may be on account of the greater relative deformation of the narrower muscle representation. The relative uniformity of the displacement and von Mises stress suggest that the different 3-D representations of muscle geometry are able to capture similar phenomena. These initial findings suggest that 3-D muscle representation, be it a bulk, CLOA or spline, may be equally valid when simulating displacement and von Mises stress distribution, and therefore human motion as well. The ultimate displacement and deformation of the moving bone was strikingly similar.

In Phase II, the level of complexity is increased with the simple mathematical geometry being replaced by the organic biological geometries of a human joint.

CHAPTER 3:

PHASE II AND PHASE III: ANATOMICAL GEOMETRY

Abstract

Phase I was a pilot study examining a muscle contraction simulated in a commercially available finite element analysis (FEA) software package using very simple geometry as a stand-in for anatomical structures. This was done with a basic geometry of two cubes (representing bone) connected by one central bar (representing the muscle) with representative tendons. Phase II increased the complexity by replacing the simple geometries with actual anatomical geometries: the scapula, humerus and teres minor. Phase III furthered the complexity by adding the remaining muscles of the rotator cuff to the model. The teres minor, supraspinatus, infraspinatus and subscapularis muscles are each represented as a lump model, a central cylinder model and a series of splines. Each representation of the muscles was then contracted using two methods. The first method used the physiological cross-sectional area to determine the maximum Force in agreement with the Hill mathematical formula and allowed the maximal forces to determine the resulting contraction. The same amount of force was applied in each case. The second method utilized a prescribed displacement of 50% of the muscles' length. The resulting von Mises stresses and overall displacement were compared to

see if there was any statistical difference between the three different representations of muscle contraction. The total time for each scenario was recorded to test for time efficiency. Two additional simulations were run for Phase III. This included a 10%+/- adjustment to the Young's modulus and Possion's ratio of each material property as well as a simulated injury of a partial tear of each of the muscles of the rotator cuff using the spline muscle representation. Comparisons were made against the original results of Phase III to test for significance.

Introduction

Skeletal muscle is one of the major areas of interest in the study biomechanics and human motion studies. Skeletal muscles have the ability to generate their own force and do not rely on external forces to create strain and deformation. Several muscle models exist that attempt to describe the mechanical behaviors of skeletal muscle. These muscle models are built around either the Hill or Huxley mathematical models for muscle contraction.[19,20] The Hill model is what is predominantly in biomechanical studies.[21] Research on the modeling of force-length relationships, force-velocity relationships and physiological (or anatomical) cross-sectional area has provided mathematical tools to assist the simulation of skeletal muscle contraction.[21, 22, 52-58]

The mathematical representation of skeletal muscle, has been used in conjunction with a variety of two-dimensional (2-D) and three-dimensional (3-D) representations of muscle geometries. 3-D muscle geometry has been represented as a lump or bulk

model, a cylinder representing a central line of action (CLOA) (or a small number working in conjunction) or a series of splines representing the direction of muscle fibers.[21,57-59]

In an effort to test the different 3-D representations of skeletal muscle, this study was undertaken to directly compare the bulk, CLOA and spline muscle geometries. Phase II of this study applied the three different ways to represent muscle by applying them to the teres minor in conjunction with the scapula and humerus. The teres minor is represented as a lump model, a central cylinder model and a series of splines. The geometry of the scapula and humerus remain unchanged throughout this phase. Two methods to simulate contraction were conducted. For one method, each representation of the muscle contracted Hill mathematical formula utilizing the physiological cross-sectional area (PCSA) to calculate the maximum force (Fmax). The same amount of force was applied in each case. The second method, prescribed a contraction of 50% the muscle length. The resulting stresses and overall displacement were compared to see if there was any statistical difference between the three different representations of muscle contraction. The total solve time for each scenario was recorded to test for time efficiency. The differences in the displacement between the two contraction methods were also compared.

For Phase III, the entire musculature of the rotator cuff (consisting of the Supraspinatus, Infraspinatus, Subscapularis and Teres Minor) was created. The maximum force and prescribed displacement methods to simulate contraction were conducted. The resulting

stresses and overall displacement were again compared to see if there was any statistical difference between the three different representations of muscle contraction. The total solve time for each scenario was recorded to test for time efficiency. The differences in the displacement between the two contraction methods were also compared.

Materials and Methods

Data Set

The anatomy for this study was created based on the National Library of Medicine's (NLM) Visible Human Male (VHM) dataset from the Visible Human Project. The entire dataset is available for download upon request from the NLM's website.[28] In total, the dataset consists of 1,878 slices as a tagged image file format (tiff) each with a resolution of 1760 x 1024. Each slice is 1 millimeter thick with a pixel size of 0.3528 millimeters. The slices are numbered in a fashion ranging from 1,001 to 2,878. A segmented set of the VHM dataset was made available and utilized to facilitate the creation of 3-D geometries. The initial segmentation was conducted by hand in Adobe's *Photoshop.* Every structure segmented was assigned its own red, green and blue (RGB) value. This was a lengthy process that took a number of hands a considerable amount of time. An example of an original image and a segmented image can be seen in Figures 3.1 and 3.2 respectively.
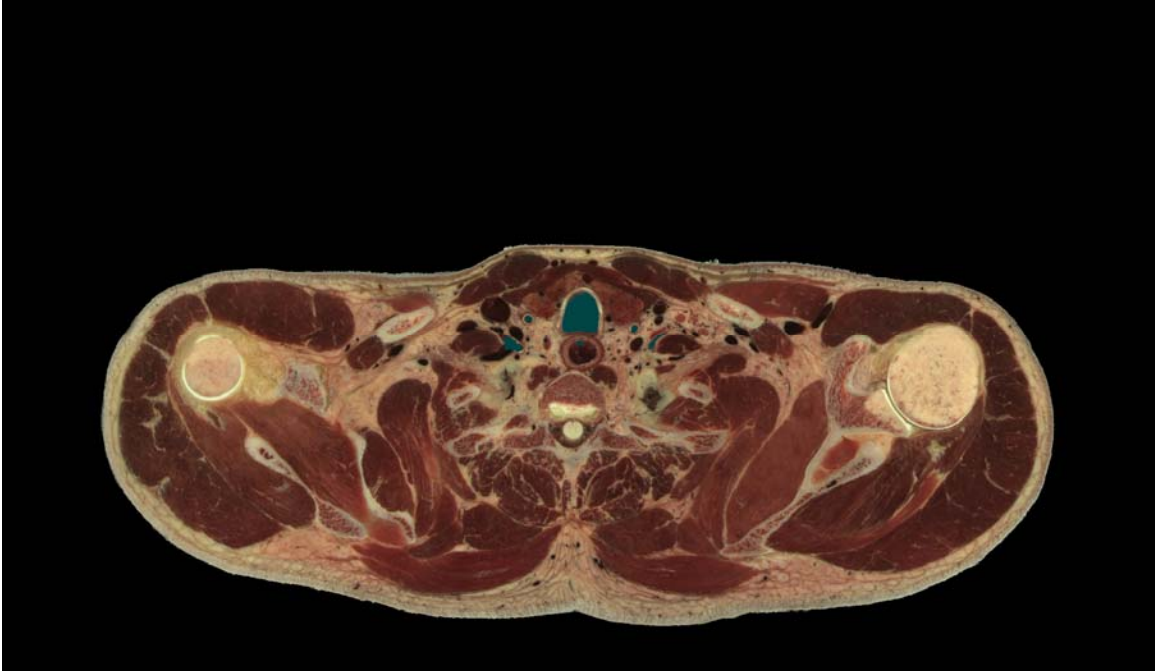
Figure 3.1: Unsegmented slice 1300 of the Visible Human Male. (Courtesy of National Library of Medicine: Public Domain)
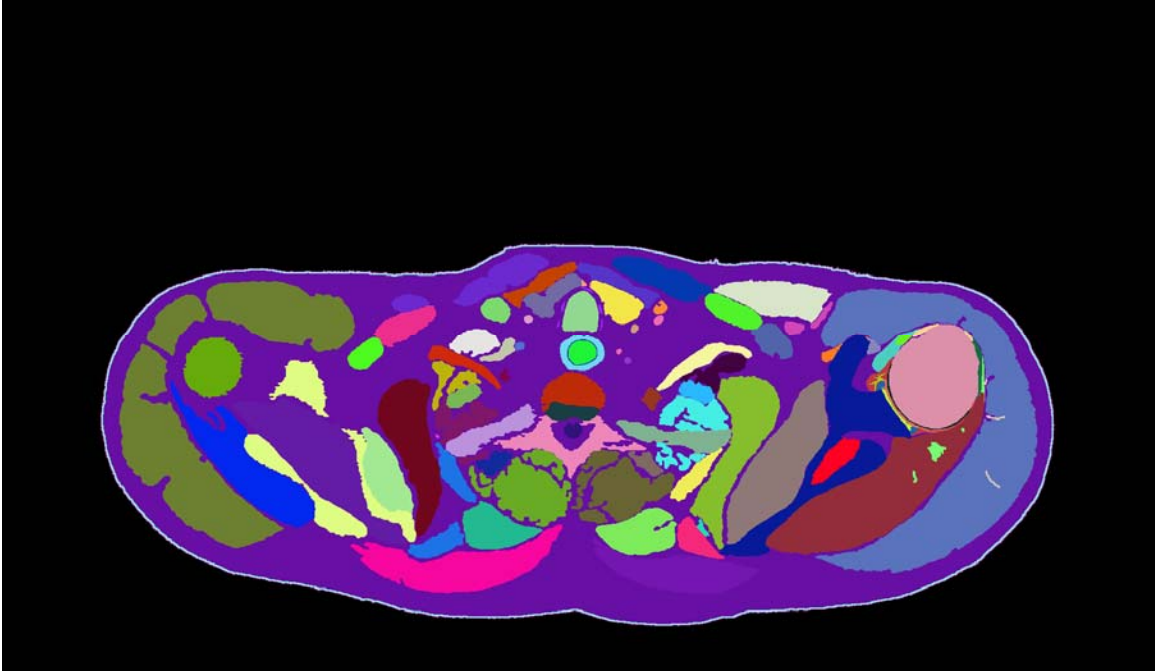
Figure 3.2: Segmented slice 1300 of the Visible Human Male. (Courtesy of Dr. Don R. Hilbelink)

Models

The 3-D geometry was created via a multistep process within the volume rendering software package *Mimics* by Materialise. The image slices relevant to the scapula, humerus and the associated structures of the rotator cuff were imported into *Mimics*. This range began with image 1260 and extended through 1610 for a total of 351 images. For Phase II only the teres minor needed to be modeled. However for Phase III, the remaining muscles of the rotator cuff were also modeled. Due to their close proximity, interrelationship and influence the geometries have on each other, the supraspinatus, infraspinatus and subscapular had to be modeled simultaneously to prevent erroneous mesh overlaps and intersections.

Initially, the segmented data set was imported into *Mimics*. The scapula, humerus, rotator cuff muscles and their associated tendons were isolated and 3-D models were created. These initial models were rough and it was decided that some further refinement to the segmentation was warranted. These models were exported as stereolithographs (STLs) for further refinement. Figure 3.3 contains an example of some of the initial "rough" results from the segmented muscle set.

Secondly, an unsegmented VHM dataset was imported into *Mimics*. The STLs of the geometries of interest were imported into this *Mimics* file. Masks were generated from the imported geometries to use as a guide and a springboard to improve on the segmentation. The resulting masks were edited and new 3-D models were generated.

Figure 3.4 contains an example of the segmentation editing. This editing involved the removal or addition of pixels that belong to their respective structures. These models, once again, were exported as STLs so they could be imported into the software package *3-Matics* (Materialise) for remeshing and further mesh cleanup.
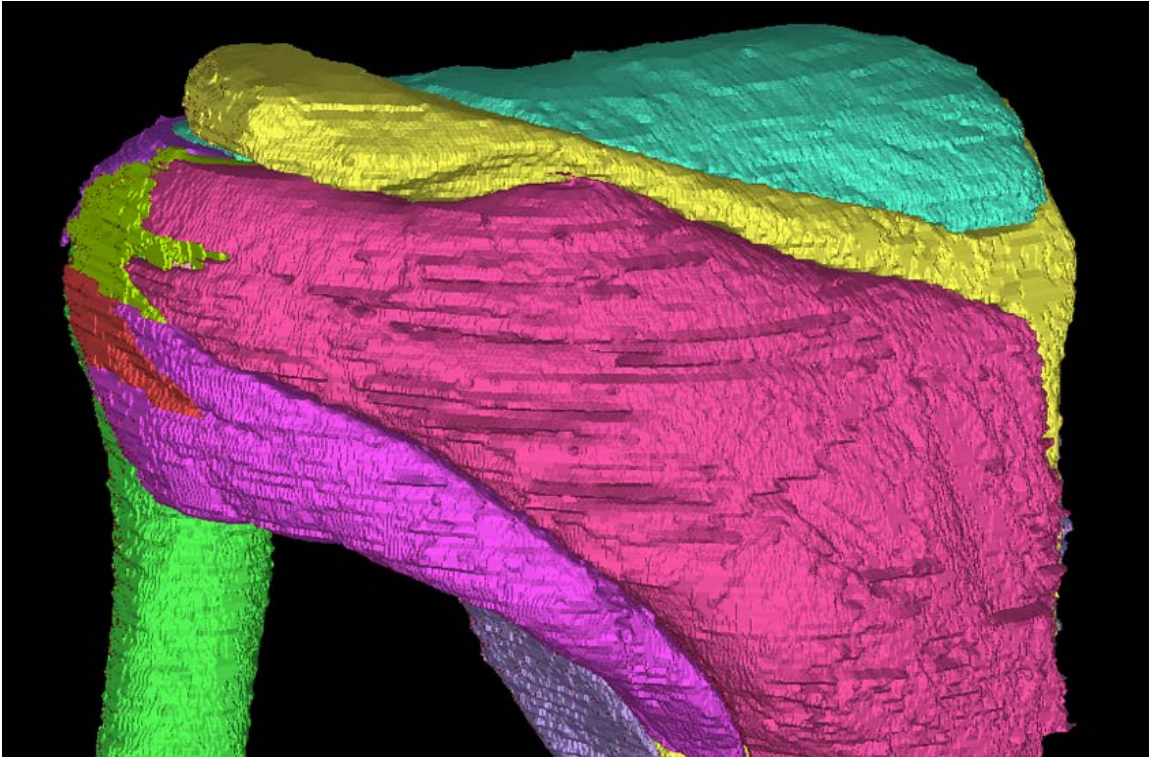
Figure 3.3: Initial rough geometry.

Mesh clean up began with the wrapping of each geometry individually. This process closes any holes that may be present and makes a watertight mesh. Further cleanup involved the searching for and subsequent removal of any overlapping or intersecting triangles. Once the initial cleanup was completed, the CLOA and the spline geometries were created using each muscle's bulk model as a base. The bulk, CLOA and spline geometries were connected to the scapula and humerus as a non-manifold mesh.
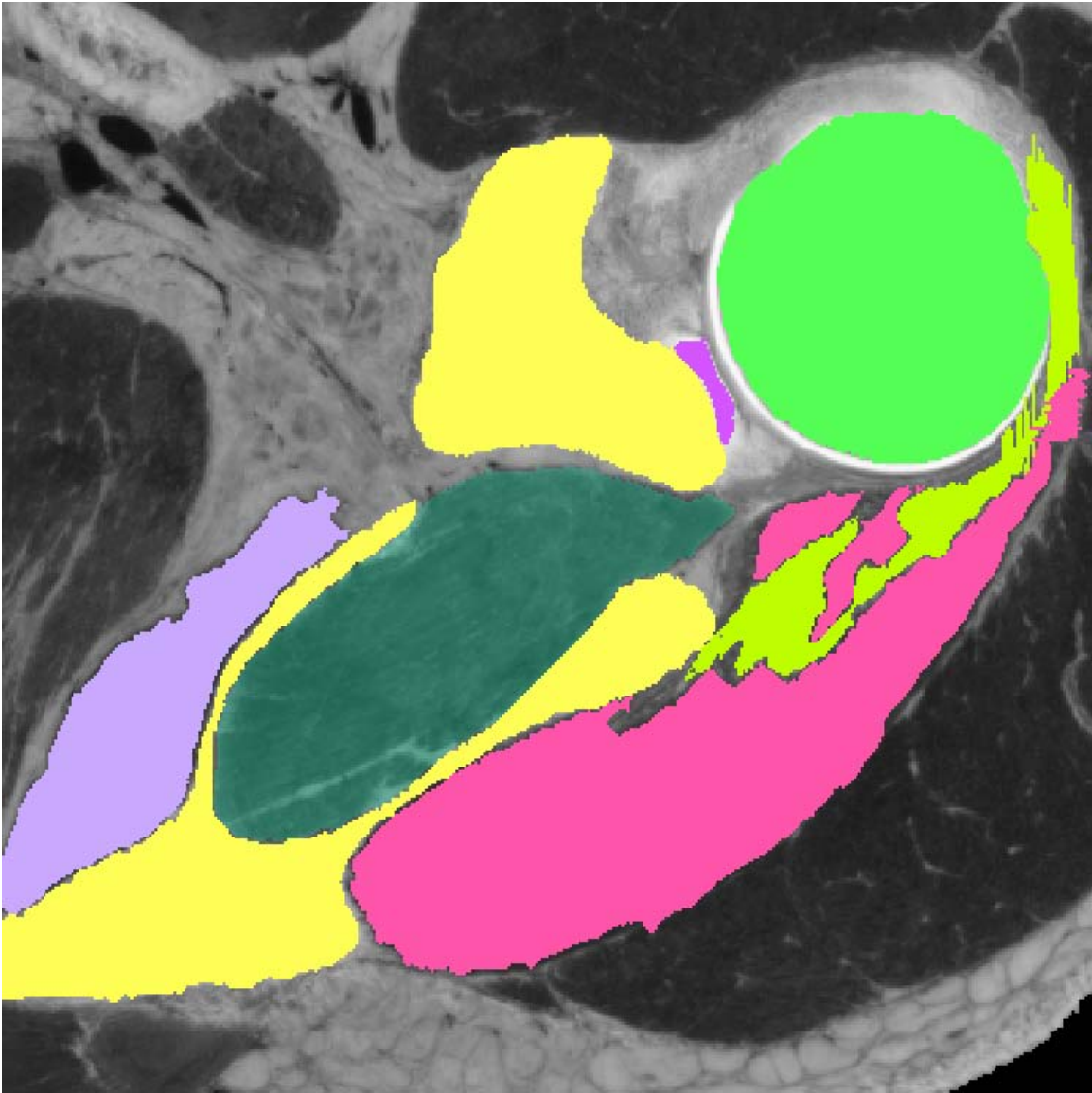
Figure 3.4: Segmentation, mask editing and cleanup

The CLOA for all muscles had a radius of 1.25 mm. The splines for all muscles had a radius 0.5 mm each. CLOA and spline representations were straight for muscles. The CLOA and spline representations for tendons curved along the path of the tendon. The representative tendons for the CLOA scenario were placed at the centroid of the

respective tendon's insertion, with muscles extending from the musculotendon interface to the centroid of the origin. Tendons for splines were placed at the centroid of the insertion and then spaced evenly at 4 mm apart along the insertion footplate. The number of splines used was dictated by the size of the footplate of their respective insertion. The insertion footplate size was the limiting factor in spline density and number on account of the size disparities between the origin surface area and the insertion surface area. Splines representing the muscle extended from the musculotendon interface and were distributed along the surface representing the origin. The teres minor has 7 splines. The supraspinatus has 12 splines. The infraspinatus has 6 splines. The subscapularis has 14 splines. Origin and insertion locations for each representative muscle was determined from personal knowledge, the VHM dataset as well as experimental results found in literature.[68,69]

Each model was subjected to further analysis, quality control and remeshing. This final model clean up began with a Triangle Reduction filter which had a geometrical error of 0.05 mm. Once these steps were complete, the model was then inspected for any intersecting or overlapping triangles. Any errors in mesh quality were fixed. Each model then underwent a series of processing steps involving: auto-remeshing and quality reduction of triangles of the geometry both had a geometrical error of 0.05 mm and a maximum triangle edge length of 10mm. The overall model was inspected a final time for intersecting or overlapping triangles and then converted into a volumetric mesh which also controlled for a maximum triangle edge length of 10 mm. The multiple checks for intersecting and overlapping triangles were performed as redundancy

measures on account that volumetric remeshing is impossible if they are present. A representative image of the bulk, CLOA and spline geometries of Phase II can be seen in Figure 3.5. A similar representative image of Phase III can be seen in Figure 3.6.

Calculations

For Phase II and Phase III, musculotendon properties were gathered from experimental data found in literature and the 3-D model itself. This included the optimal muscle fiber lengths and pennation angles (alpha).[70-72] Fmax was calculated using the PCSA * Muscle Specific Tension. The muscle specific tension (or muscle stress constant) was assumed to be 33 N/cm^2.[21,70] PCSA is calculated as the volume of the muscle divided by the optimal fiber length. The volumes of the teres minor, supraspinatus, infraspinatus and subscapularis were captured from the mesh geometry. The data was entered into the Hill equation $(v + b) + (F + a) = b(F_{max} + a)$ and resulted in the stereotypical force-velocity and power-velocity curves.[19,21,58] Muscle contraction was simulated for Fmax generation. Thereby the muscle was at its' highest level of contraction and the contraction velocity was zero. Since the muscle pathways are off the x,y,z axes, cosine values for the force vectors were calculated for the bulk, CLOA and spline scenarios. Tables 3.1, 3.2, 3.3 and 3.4 contain summaries of the numeric data for the teres minor, supraspinatus, infraspinatus and subscapularis respectively.
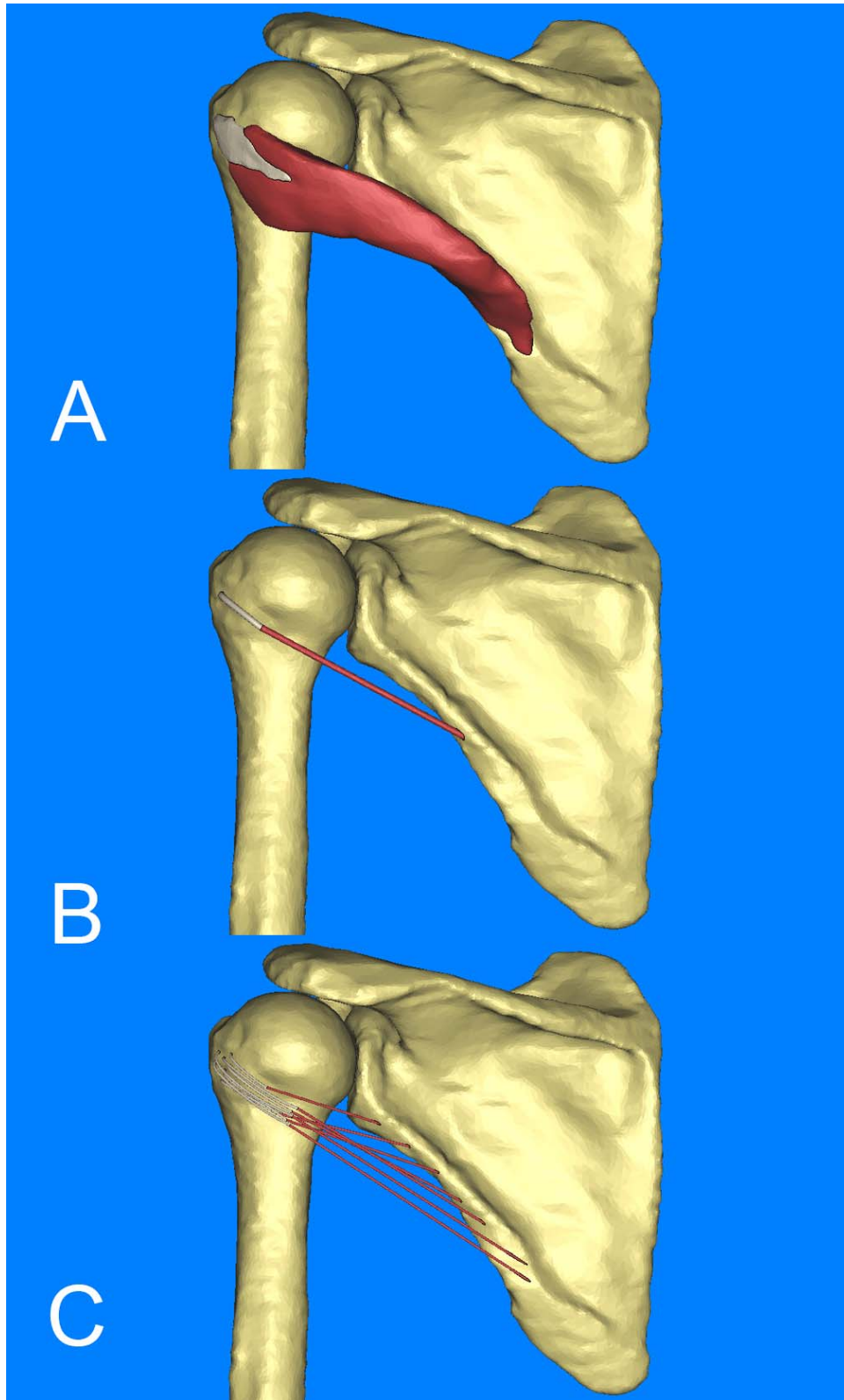
Figure 3.5: Representative lump (A), central line of action (B) and spline (C) geometries of Phase II, teres minor.
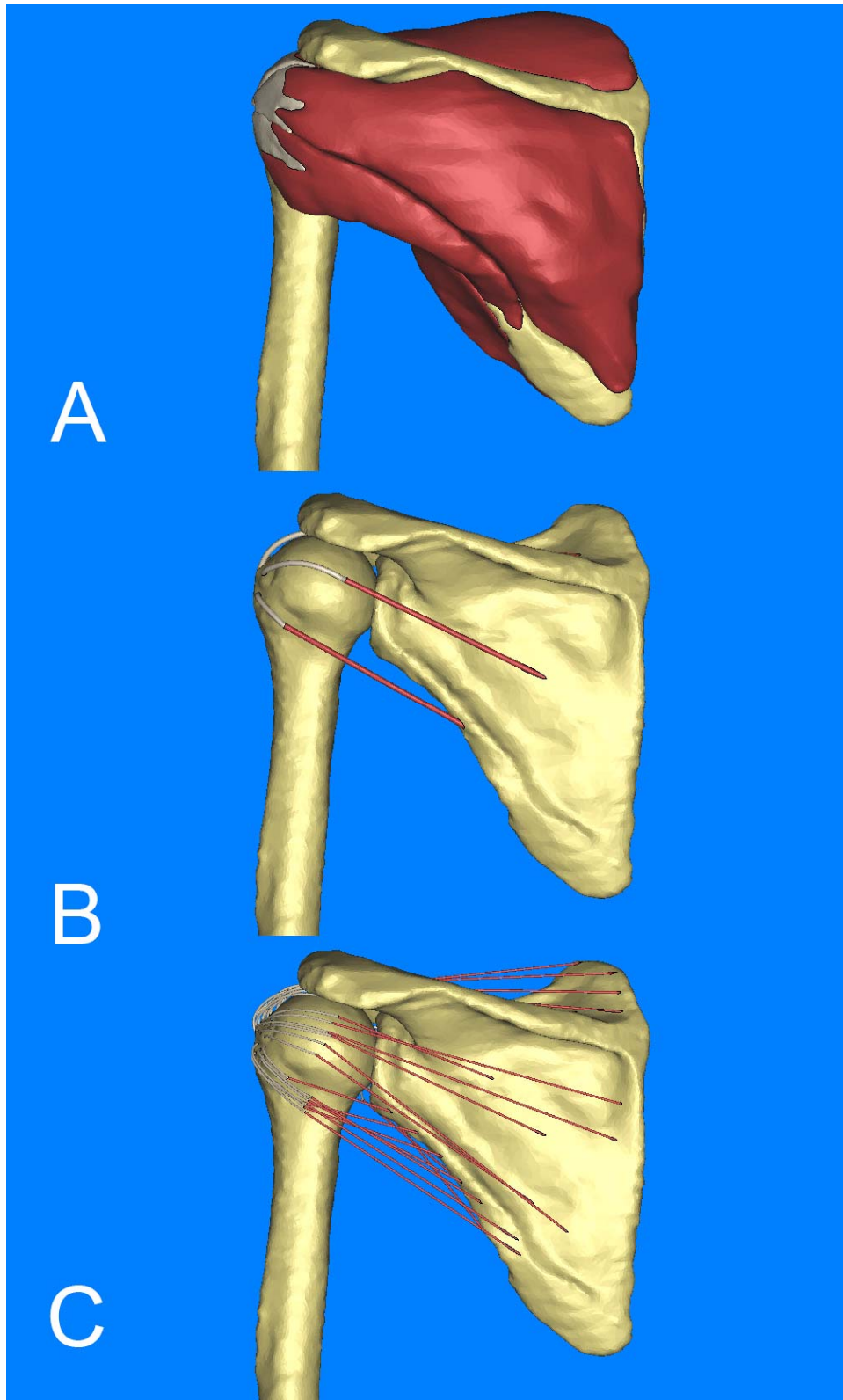
Figure 3.6: Representative lump (A), central line of action (B) and spline (C) geometries of Phase III, supraspinatus, infraspinatus, teres minor and subscapularis.

Table 3.1: Teres Minor Musculoskeletal Numeric Data

Teres Minor Muscle Architecture					
Volume	Opt. F. L.	PCSA	Sp. Ten.	Fmax	
cm^3	cm	cm^2	N/cm^2	N	
47.91	5.72	8.38	33	276.40	
Bulk and CLOA cosines and force vectors					
	Cosine α	X force	Cosine β	Y force	Cosine γ	Z force
Bulk/CLOA	0.6376	176.24	-0.5991	-165.59	0.4842	133.83
Spline cosines and force vectors					
	Cosine α	X force	Cosine β	Y force	Cosine γ	Z force
Spline 1	0.7838	216.64	-0.5199	-143.70	0.3395	93.84
Spline 2	0.7812	215.92	-0.5605	-154.92	0.2747	75.93
Spline 3	0.7632	210.95	-0.5396	-149.15	0.3554	98.23
Spline 4	0.6944	191.93	-0.5288	-146.16	0.488	134.88
Spline 5	0.6657	184.00	-0.5112	-141.30	0.5436	150.25
Spline 6	0.6503	179.74	-0.5213	-144.09	0.5526	152.74
Spline 7	0.6273	173.39	-0.5428	-150.03	0.5585	153.37

Table 3.2: Supraspinatus Musculoskeletal Numeric Data

Supraspinatus Muscle Architecture					
Volume	Opt. F. L.	PCSA	Sp. Ten.	Fmax	
cm^3	cm	cm^2	N/cm^2	N	
88.23	3.28	13.05	33	680.28	
Bulk and CLOA cosines and force vectors					
	Cosine α	X force	Cosine β	Y force	Cosine γ	Z force
Bulk/CLOA	0.7797	530.41	-0.621	-422.45	0.08	53.42
Spline cosines and force vectors					
	Cosine α	X force	Cosine β	Y force	Cosine γ	Z force
Spline 1	0.8957	609.33	-0.4412	-300.14	-0.0549	-37.35
Spline 2	0.8265	562.25	-0.5344	-363.54	0.1772	120.55
Spline 3	0.8424	573.07	-0.5226	-355.51	0.1318	89.66
Spline 4	0.857	583.00	-0.5152	-350.48	-0.011	-7.48
Spline 5	0.7675	522.11	-0.6368	-433.20	0.0735	50.00
Spline 6	0.8412	572.25	-0.5394	-366.94	0.0389	26.46
Spline 7	0.8144	554.02	-0.573	-389.80	0.0915	62.25
Spline 8	0.7885	536.40	-0.5925	-403.07	0.165	112.25
Spline 9	0.6881	468.10	-0.6796	-462.32	0.2542	172.93

Table 3.2 Continued

Spline 10	0.7577	515.45	-0.6468	-440.01	0.0867	58.98
Spline 11	0.7224	491.43	-0.6886	-468.44	0.063	42.86
Spline 12	0.759	516.33	-0.6503	-442.39	0.0335	22.79

Table 3.3: Infraspinatus Musculoskeletal Numeric Data

Infraspinatus Muscle Architecture					
Volume	Opt. F. L.	PCSA	Sp. Ten.	Fmax	
cm^3	cm	cm^2	N/cm^2	N	
225.01	6.76	33.29	33	1098.42	
Bulk and CLOA cosines and force vectors					
	Cosine α	X force	Cosine β	Y force	Cosine γ	Z force
Bulk/CLOA	0.6956	764.06	-0.5589	-613.91	0.4513	495.72
Spline cosines and force vectors					
	Cosine α	X force	Cosine β	Y force	Cosine γ	Z force
Spline 1	0.7822	859.18	-0.4708	-517.14	0.4081	448.27
Spline 2	0.7968	875.22	-0.5266	-578.43	0.2963	325.46
Spline 3	0.7671	842.60	-0.5192	-570.30	0.3769	413.99
Spline 4	0.7325	803.59	-0.514	-563.59	0.4463	490.22
Spline 5	0.6068	666.52	-0.49	-538.23	0.6259	687.50
Spline 6	0.6496	713.53	-0.485	-532.73	0.5851	642.69

Table 3.4: Subscapularis Musculoskeletal Numeric Data

Subscapularis Muscle Architecture					
Volume	Opt. F. L.	PCSA	Sp. Ten.	Fmax	
cm^3	cm	cm^2	N/cm^2	N	
262.24	8.92	29.40	33	970.17	
Bulk and CLOA cosines and force vectors					
	Cosine α	X force	Cosine β	Y force	Cosine γ	Z force
Bulk/CLOA	0.4304	417.56	-0.8427	-817.56	0.3236	313.95
Spline cosines and force vectors					
	Cosine α	X force	Cosine β	Y force	Cosine γ	Z force
Spline 1	0.6432	624.01	-0.48	-465.68	-0.1635	-158.62
Spline 2	0.5464	530.10	-0.8201	-795.64	-0.1697	-163.64
Spline 3	0.5164	501.00	-0.8552	-829.69	-0.0441	-42.78
Spline 4	0.4541	440.55	-0.8523	-826.88	0.2597	251.95
Spline 5	0.3954	383.61	-0.8004	-776.52	0.4505	437.06

Table 3.4 Continued

Spline 6	0.5172	501.77	-0.85	-823.64	0.0996	96.63
Spline 7	0.5066	491.49	-0.8622	-836.48	0.0058	5.63
Spline 8	0.4579	443.24	-0.8448	-819.60	0.2769	268.64
Spline 9	-0.8656	-839.78	-0.478	-463.74	0.149	143.56
Spline 10	0.3686	357.60	-0.7183	-696.87	0.5901	572.50
Spline 11	0.3748	363.62	-0.7982	-773.39	0.4715	457.44
Spline 12	-0.2731	-264.95	0.6784	658.16	-0.682	-661.66
Spline 13	0.3627	351.88	-0.7686	-745.67	0.527	511.28
Spline 14	-0.5401	-529.28	0.841	824.16	0.019	18.42

COMSOL

A 3-D solid Structure mechanics module was used for the muscle contraction. A step function was used as the basis for the applied force. The idea was to capture the muscle as it held and maintained its most contracted state (velocity = 0 at F=Fmax). Upon the completion of the geometric modeling, the surface and volume meshes were then exported as MPHTXT files, the *COMSOL* ready mesh format. With the mesh imported, material properties were assigned to the relative geometries. The representative bones were given a Young's modulus of 1.0×10^{10} Pa, a Poisson's ratio of 0.3 and a density of 2570 kg/m^3.[60] The representative muscle was given a Young's modulus of 1.162×10^6 Pa, a Poisson's ratio of 0.4 and a density of 1056 kg/m^3.[60] The tendon was given a Young's modulus of 1.6×10^6 Pa, a Poisson's ratio of 0.497 and a density of 1670 kg/m^3.[61] The scapula was constrained to serve as the nonmoving aspect of the shoulder joint. Contact pairs were created so the bones, muscles and tendons would interact and collide with one another. Boundary loads were applied in Newtons for the Bulk scenario. Normalized boundary loads (Force/PSCA) were applied as force per unit area for the CLOA and Spline scenarios to account for the geometries'

smaller diameters. The forces were applied along the x, y and z axes according to the relative cosine α, β, or γ of the geometry. The model was then solved and displacement and von Mises stress were collected. Solution time data was also collected. This was done for the bulk, CLOA and spline models for Phase II and Phase III. The distance displacement was measured on the most inferior point of the humerus' trochlea.[61] It was anticipated that the von Mises stresses would display that the tendon acted as a damper in force transmission from muscle to bone.[63,73] FEA analysis with *COMSOL* was run on a Dell Precision T7500 with an Intel Xeon CP X5690 @ 3.47 GHz and 96 GB of RAM.

However unlike Phase I, *COMSOL* was unable to resolve a solution to any scenario for Phase II or Phase III. The default error threshold prevented *COMSOL* from prevented a solution. With the error thresholding removed, the results became anatomically impossible. The solve times, displacement and von Mises stress could not be established. Troubleshooting was undertaken to resolve this issue.

Alternative Attempts

To address the unexpected behavior of the phase scenarios, alterations to the model were conducted. A sphere with a 5 mm radius at the centroid of the humeral head was created. This sphere was fixed in place to provide a center of rotation for the model. Additionally, the way the muscle contraction was modeled was also examined. Two

scenarios, one involving the application of the Fmax to the muscle and one involving limiting the range of muscle contraction by prescribed displacement were conducted.

The model was meshed and volumized in 3-matic and then exported into *COMSOL*. Once the mesh was imported contact pairs for the sphere were established. The internal sphere was made stationary as was the scapula. Forces were placed on the boundary between the tendon and the muscle to allow for muscle contraction. Similar to the initial attempt, muscle contraction was simulated for Fmax generation. The calculations in Tables 3.1, 3.2, 3.3 and 3.4 contain values that were used as the applied forces for Phase II and Phase III.

An additional scenario of limiting the length of contraction was used. A prescribed displacement for Phase II and Phase III simulated a 50% shortening of each muscle. It was decided to use 50% since several sources provided a range of contraction from 30% to 70% of a muscles resting length.[65-67] The midpoint for each muscle were calculated as an x,y,z value and distance value for the bulk, CLOA and spline scenarios. Tables 3.5, 3.6, 3.7 and 3.8 contain summaries of the numeric data for the teres minor, supraspinatus, infraspinatus and subscapularis respectively.

Table 3.5: Teres Minor Prescribed Displacement Data

Bulk and CLOA Shortening Distance (mm)			
	Delta X	Delta Y	Delta Z
Bulk/CLOA	-27	25.37	-20.5
Spline Shortening Distance (mm)			
	Delta X	Delta Y	Delta Z
Spline 1	-17.53	11.63	-7.6
Spline 2	-20.32	14.58	-7.14
Spline 3	-23.23	16.42	-9.32
Spline 4	-25.22	19.11	-17.72
Spline 5	-29.11	21.2	-22.54
Spline 6	-33.32	28.81	-29.66
Spline 7	-32.03	25.68	-27.22

Table 3.6: Supraspinatus Prescribed Displacement Data

Bulk and CLOA Shortening Distance (mm)			
	Delta X	Delta Y	Delta Z
Bulk/CLOA	-27	25.37	-20.5
Spline Shortening Distance (mm)			
	Delta X	Delta Y	Delta Z
Spline 1	-41.22	20.3	2.53
Spline 2	-22.09	14.28	-4.74
Spline 3	-32.41	20.1	-5.07
Spline 4	-48.08	28.9	0.62
Spline 5	-36.48	30.26	-3.49
Spline 6	-48.13	30.86	-2.23
Spline 7	-22.5	22.22	-8.31
Spline 8	-32.24	24.22	-6.74
Spline 9	-47.52	33.43	-5.36
Spline 10	-34.84	29.74	-3.99
Spline 11	-15.59	14.9	-1.37
Spline 12	-24.2	20.84	-1.09

Table 3.7: Infraspinatus Prescribed Displacement Data

Bulk and CLOA Shortening Distance (mm)		
Delta X	Delta Y	Delta Z
Bulk/CLOA	-29.9	24	-19.39

Spline Shortening Distance (mm)		
	Delta X	Delta Y	Delta Z
Spline 1	-27.1	16.3	-14.1
Spline 2	-50	33.14	-18.65
Spline 3	-49.08	33.22	-24.15
Spline 4	-35.5	24.91	-21.63
Spline 5	-38.6	31.17	-39.82
Spline 6	-35.21	26.32	-31.72

Table 3.8: Subscapularis Prescribed Displacement Data

Bulk and CLOA Shortening Distance (mm)		
Delta X	Delta Y	Delta Z
Bulk/CLOA	-21.48	42.06	-16.16

Spline Shortening Distance (mm)		
	Delta X	Delta Y	Delta Z
Spline 1	27.92	-32.47	-7.1
Spline 2	17.82	-26.75	-5.56
Spline 3	20.69	-34.26	-1.77
Spline 4	27.13	-42.21	-0.95
Spline 5	24.5	-46	14.01
Spline 6	37.37	-63.6	0.43
Spline 7	22.27	-36.61	4.29
Spline 8	23.89	-48.36	27.22
Spline 9	21.95	-40.51	13.28
Spline 10	21.27	-36.85	5.37
Spline 11	20.4	-43.46	25.67
Spline 12	14.79	-31.33	21.48
Spline 13	23.11	-45.04	37
Spline 14	16.1	-39.99	40.2

Additionally, to examine if the effect of the different geometries was consistent regardless of material properties, scenarios were run for a 10% increase and a 10%

decrease in the Young's modulus and Poisson's ratio. This experiment examined the effect of a more and less stiff material behaved under contraction. For the stiffer scenario, the Young's moduli for the bone, muscle and tendon were increased to 1.0×10^{11} Pa, 1.162×10^7 Pa, and 1.6×10^7 Pa and the Poisson's ratio reduced to 0.27, 0.36 and 0.4473 respectively. For the less stiff experiment the Young's moduli for the bone, muscle and tendon were decreased to 1.0×10^9 Pa, 1.162×10^5 Pa, and 1.6×10^5 Pa respectively. The Poisson's ratio increased to 0.33 for bone, 0.44 for muscle but stayed at 0.497 for tendon on account the maximum limit to a Poisson's ratio value is 0.5. The density of each material remained the same throughout the two experiments. Contraction from the application of Fmax and prescribed displacement was then conducted. Displacement, von Mises stress and solve time was recorded for comparison.

Additionally, a simulated injury was conducted utilizing the spline muscle representation. The number of splines representing each muscle was reduced by one-third. The numbers of splines reduced was rounded down as mathematically necessary. Teres minor was reduce from 7 to 5 splines. Infraspinatus was reduced from 6 to 4 splines. Supraspinatus was reduced from 12 to 8 splines. Subscapularis was reduced from 14 to 10 splines. The splines were removed superiorly/anteriorly in a systemic fashion for each structure so that each muscle had a representative partial "tear." The applied force and prescribed displacement were applied to mimic the muscle contraction. The resulting data was compared against the "uninjured" spline results.

Results

Initial Attempts at Phase II and III Muscle Contraction

Three different scenarios of each muscle were created. The different representations consisted of a bulk, CLOA, and spline constructions. The meshes for each representation of Phase II had 204,092, 133,384 and 270,500 tetrahedral elements respectively. The meshes for each representation of Phase III had 374,065, 159,620 and 845,083 tetrahedral elements respectively. Each mesh successfully imported into *COMSOL*. However, using default convergence error thresholds no scenarios for Phases II or III were solvable. When these error safeguards were removed, the resulting values for displacement and von Mises stress were well beyond anything anatomically possible. A representative image showing an almost 2 meter level of displacement with bizarre levels of deformation can be seen in Figure 3.7.

Alternative Attempts at Phase II and III Muscle Contraction

In addition to the muscle of the rotator cuff, the shoulder joint also have several other structures, such as ligaments and cartilage that help keep the humeral head in the joint socket. These structures limit the joint and help maintain the center of rotation. An internal sphere at the centroid of the humeral head was added. Anatomically, this sphere serves to keep the humeral head within the joint as a stand in for the ligaments

that would make up the joint capsule. This internal sphere serves as a center of rotation for the humerus.
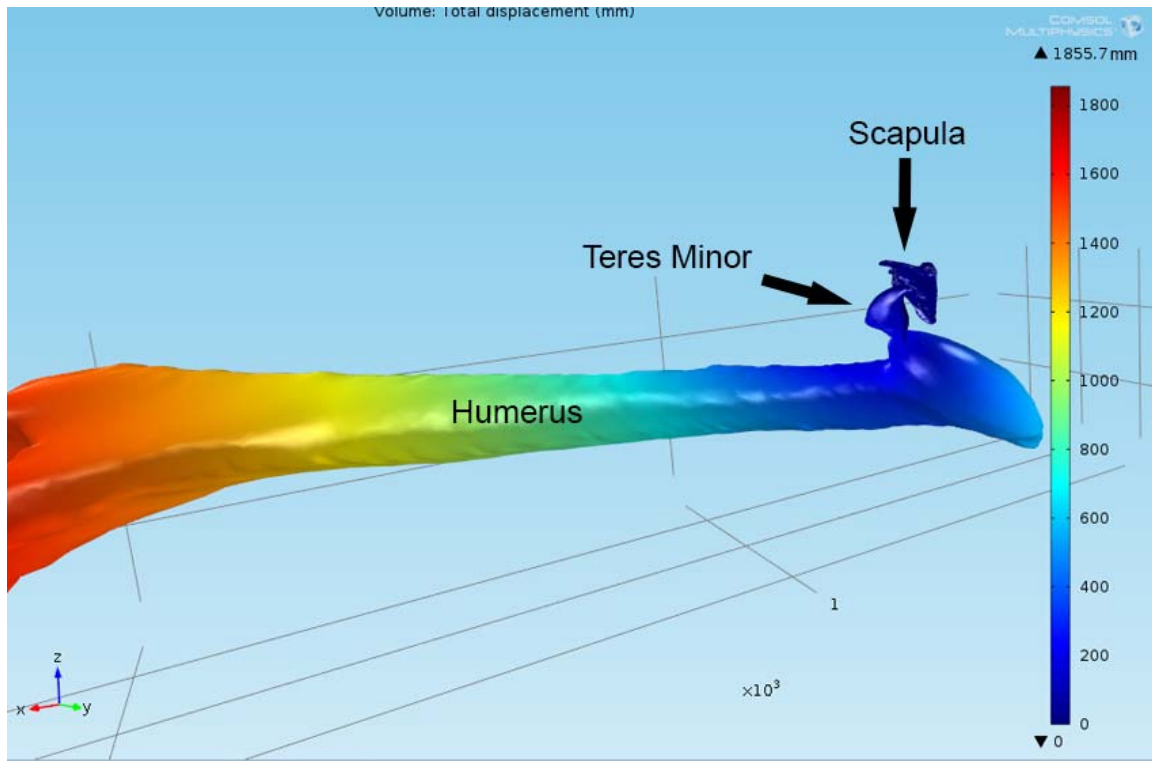
Figure 3.7: Anatomically impossible results with error threshold removed

The addition of internal sphere slightly altered the tetrahedral count for each Bulk, CLOA and Spline mesh. The meshes for each representation of Phase II had 203,533, 143,815 and 263,524 tetrahedral elements respectively. The meshes for each representation of Phase III had 376,209, 170,070 and 851,575 tetrahedral elements respectively. Each mesh successfully imported into *COMSOL* and successfully solved for both Fmax and prescribed displacement. For comparative purposes, measurements were taken at the same point (the tip of the trochlea) which can be seen in Figure 3.8. Table 3.9 contains the numerical data for displacement and von Mises for each scenario

of Phase II. Table 3.10 contains the numerical data for displacement and von Mises stress for each scenario of Phase III. Table 3.11 contains data comparing the initial findings of Phase III with the more and less stiff scenarios. Table 3.12 contains data comparing the original data of the non-injured spline model for Phase III against the injured data.
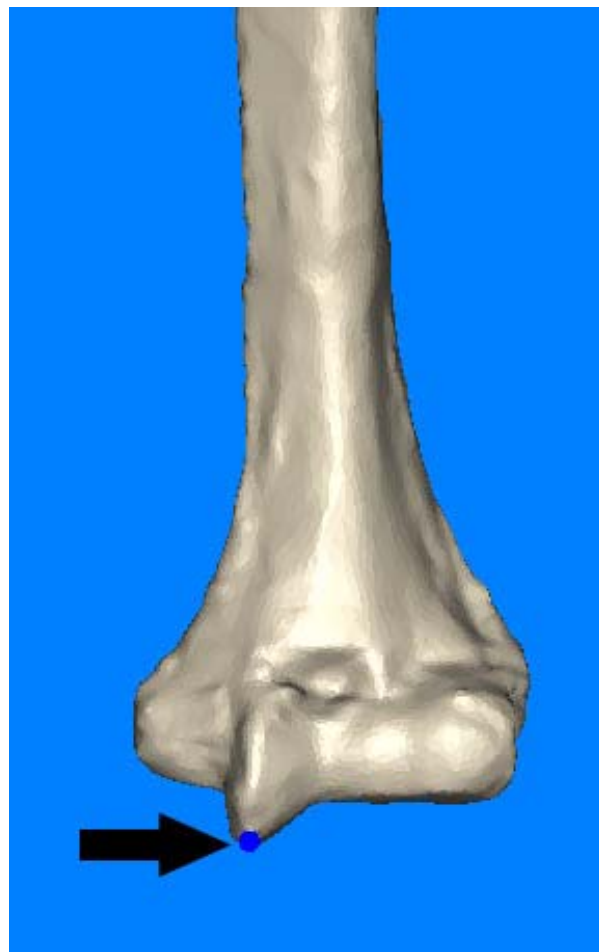
Figure 3.8: Measurement Point

Table 3.9: Phase II: Teres Minor Results Data

Resultant Displacement from Prescribed Displacement (mm)					
Muscle Type	X	Y	Z	Time	Von Mises (N/m2)
Bulk	0.69	0.27	0.06	1 h 9' 42"	3.43x10e10
CLOA	0.76	1.81	0.17	13' 12"	1257.1
Spline	1.01	3.04	0.11	2 h 56' 4"	3.678x10e10
Resultant Displacement from Applied Force (mm)					
Muscle Type	X	Y	Z	Time	Von Mises (N/m2)
Bulk	1.19	2.12	0.24	1 h 33' 56"	7.5x10e10
CLOA	0.92	0.62	0.02	14' 16"	1.3x10e25
Spline	1.78	2.13	0.40	6 h 32' 17"	2.55x10e10

Table 3.10: Phase III: Rotator Cuff Results Data

Resultant Displacement from Prescribed Displacement (mm)					
Muscle Type	X	Y	Z	Time	Von Mises (N/m2)
Bulk	0.03	0.75	0.01	2 h 30' 54"	2.73x10e13
CLOA	2.61	1.20	0.40	38' 3"	9.7x10e9
Spline	2.10	1.76	0.53	7 h 7' 12"	1.47x10e12
Resultant Displacement from Applied Force (mm)					
Muscle Type	X	Y	Z	Time	Von Mises (N/m2)
Bulk	1.84	3.15	0.91	5 h 15' 36"	5.68x10e12
CLOA	0.54	1.81	0.11	46' 52"	1.64x10e10
Spline	3.43	5.40	0.44	10 h 22'12"	3.61x10e13

Table 3.11: Phase III: Rotator Cuff with Variable Material Properties

Scenario[a,b]	X (mm)	Y (mm)	Z (mm)	Time	Von Mises (N/m2)
Stiffer Material Properties					
Stiff Bulk N	0.03	0.62	0.01	3 h 11' 6"	5.66x10e12
Stiff Bulk PD	1.79	3.09	0.87	4 h 56' 31"	4.24x10e12
Stiff CLOA N	0.30	0.99	0.23	50' 6"	2.00x10e7
Stiff CLOA PD	0.62	1.80	0.10	48' 59"	4.35x10e9
Stiff Spline N	1.17	0.88	0.34	7 h 51' 3"	2.97x10e11
Stiff Spline PD	3.33	5.13	0.52	11 h 3' 27"	3.01x10e13
DIFFERENCE					
Stiff Bulk N	0.00	-0.13	0.00	+40' 12"	-2.16x10e13

Table 3.11 Continued

Stiff Bulk PD	-0.05	-0.06	-0.04	-19" 5'	-1.44x10e12
Stiff CLOA N	-2.31	-0.21	-0.17	+12' 3"	-9.68x10e9
Stiff CLOA PD	0.08	-0.01	-0.01	+2' 7"	-1.21x10e10
Stiff SPLINE N	-0.93	-0.88	-0.19	+43' 51"	-1.17x10e12
Stiff Spline PD	-0.10	-0.27	0.08	+41' 15"	-6.00x10e12
Looser Material Properties					
Loose Bulk N	0.52	1.32	0.66	3 h 24"	2.80x10e13
Loose Bulk PD	1.79	3.09	0.87	5 h 33' 31"	6.73x10e12
loose CLOA N	3.22	2.01	1.32	42' 41"	5.75x10e20
Loose CLOA PD	0.61	1.85	0.16	47' 33"	3.87x10e11
Loose Spline N	2.94	2.22	1.17	6 h 58' 3"	6.45x10e12
Loose Spline PD	3.39	5.11	0.49	10 h 55' 25"	4.38x10e13
DIFFERENCE					
Loose Bulk N	0.49	0.57	0.65	+53' 6"	+7.00x10e11
Loose Bulk PD	-0.05	-0.06	-0.04	+17' 55"	+1.05x10e12
loose CLOA N	0.61	0.81	0.92	+4' 38"	+5.75x10e20
Loose CLOA PD	0.07	0.04	0.05	+41"	+3.51x10e11
Loose Spline N	0.84	0.46	0.64	-9' 9"	+4.98x10e12
Loose Spline PD	-0.04	-0.29	0.05	+33' 13"	+7.70x10e12

a: N = Applied Force, b: PD = Prescribed Displacement

Table 3.12: Phase III: Rotator Cuff Normal vs. Injured

Resultant Displacement from Uninjured Shoulder (mm)						
Muscle Contraction Method	X	Y	Z	Elements	Time	Von Mises (N/m2)
Spline Applied Force	2.1	1.76	0.53	851575	7 h 7' 12"	1.47x10e12
Spline Prescribed Displacement	3.43	5.4	0.44	851575	10 h 22' 12"	3.61x10e13
Resultant Displacement from Injured Shoulder (mm)						
Muscle Contraction Method	X	Y	Z	Elements	Time	Von Mises (N/m2)
Spline Applied Force	2.28	2.13	0.4	599293	5 h 38' 49"	3.31x10e12
Spline Prescribed Displacement	1.01	3.04	0.11	599293	6 h 54' 9"	6.66x10e11
Difference between Normal vs. Injured Shoulder						
Muscle Contraction Method	X	Y	Z	Elements	Time	Von Mises (N/m2)
Spline Applied Force	0.18	0.37	-0.13	-252282	-1 h 28' 23"	1.91x10e12
Spline Prescribed Displacement	-2.42	-2.4	-0.33	-252282	-3 h 28' 3"	-3.54x10e13

Discussion and Conclusions

Initial Attempts at Phase II and III Muscle Contraction

The data concerning element count and its associated increase with the addition of more complex geometries is not surprising. However, the inability to solve each simulation was unexpected. The default error threshold of *COMSOL* prevented convergence of a solution.

Troubleshooting efforts involved checking and rechecking the mathematical calculations, model scales as well as the units for each numerical value. No errors in this regard were found. The musculotendon parameters of volume, PCSA, Fmax were all compared against known applications of the VHM dataset and were comparable.[70] A table comparing the values can be found in Table 3.13. Any potential differences may be on account that Garner et al used images at 5 mm slice increments, while this study used the full 1 mm slice increments.[70] Furthermore, since many calculations are a result from the same optimal fiber length values from literature, the difference in volumes would account for the difference in the resulting PCSA and Fmax values.[71,72] A more in depth study concerning the muscle properties of the rotator cuff can be seen in Appendix A.

Table 3.13: VHM Musculotendon Numerical Property Comparison

Muscle Name	Garner et al[69]		
	Volume cm^3	PCSA cm^2	Fmax N
Teres Minor	38.7	6.77	223.35
Supraspinatus	89.23	20.8	687.84
Infraspinatus	225.36	33.32	1099.61
Subscapularis	318.52	35.69	1177.93
	This Study		
Muscle	Volume	PCSA	Fmax
Teres Minor	47.91	8.38	276.4
Supraspinatus	88.23	20.61	680.29
Infraspinatus	225.01	33.29	1098.42
Subscapularis	262.24	29.4	970.17
	Difference		
Muscle	Volume	PCSA	Fmax
Teres Minor	9.21	1.61	53.05
Supraspinatus	1	0.19	7.55
Infraspinatus	0.35	0.03	1.19
Subscapularis	56.28	6.29	207.76

It is our theory that the use of a linear elastic model may be the source of the error. Personal Communication with *COMSOL* suggested that a hyperelastic model maybe an alternative option for this particular set of geometries. The strain value being above 10% is one indication and a potential source of a lack of convergence. Furthermore, it is possible that the geometries themselves are creating singularities of very high values.[74] However, the use of a linear elastic model should still work under the circumstances of this study since the forces involved do not extend into the plasticity range.[75] Furthermore, the lack of a joint capsule allows the muscle to contract without restriction and made such dramatic deformities possible.

Future studies will include substituting the linear elastic model with a hyperelastic or viscoelastic one. Other studies have attempted this to varying levels of success.[51,57,63,76-78] Additionally, this study focused on muscles undergoing active contraction. Future study will include testing if the linear elastic model would be better suited for passive muscle interaction.

Alternative Attempts at Phase II and III Muscle Contraction

The initial examination of muscle contraction of the muscles of the rotator cuff relied solely on the muscles maintaining the center of rotation for the humeral head. However, the removal of the error threshold and the extreme and erroneous deformation implied that the representation of the muscles alone was not sufficient. A small sphere at the center of the humeral head was created as a stand in for the other ligaments and cartilage structures that contribute to defining the shoulder's center of rotation. This sphere as the center of rotation combined with the two different methods of modeling muscle contraction allowed for each scenario to solve successfully.

For Phase II the amount of variation in the displacement was very low for both scenarios when broken down to their X, Y, Z components. For the prescribed displacement scenario, the average X, Y and Z was 0.82 ± 0.17 mm, 1.71 ± 1.39 mm and 0.11 ± 0.05 mm respectively. For the applied Fmax scenario, the average X, Y and Z was 1.3 ± 0.44 mm, 1.62 ± 0.87 mm and 0.22 ± 0.19 mm respectively. The CLOA had the shortest solve time which is not surprising due to it being the simplest model.

For Phase III the amount of variation in the displacement was very low for both scenarios when broken down to their X, Y, Z components. For the prescribed displacement scenario, the average X, Y and Z was 1.58 ± 1.37 mm, 1.23 ± 0.5 mm and 0.32 ± 0.27 mm respectively. For the Applied Fmax scenario, the average X, Y and Z was 1.58 ± 1.37 mm, 1.23 ± 0.5 mm and 0.32 ± 0.27 mm respectively. Again, the CLOA had the shortest solve time which is not surprising due to it being the simplest model.

Furthermore, the values for Von Mises stress, for both Phase II and Phase III were at their peak along the interfaces of the tendon and muscles. This is as expected because any actual force originates at this muscle/tendon interface. As the muscle actively contracts, the tendon passively transmits the force to the bone.

Solve time varied drastically overall. The more complex the model, as measured as the number of tetrahedral elements and the number of boundaries that had a boundary condition, the longer the solve time which differed from an hour to several hours. This additional solve time may not be worth it as the differences for each scenario is just several millimeters. Unless certain geometries are critical to a simulation, it is our suggestion that the CLOA be used to model joint movements. It would be interesting to see if this hold true for muscles that contribute to a more dramatic movement, such as the bicep and elbow joint. It would be also interesting to add the element of time and model a timed activation and deactivation of each muscle as the rotator cuff (or any joint) worked as a unit on a temporal basis.

The examination of the role of material property stiffness went as predicted. The stiffer scenario saw a reduction in displacement and a reduction in von Mises stress. This was especially true for the contraction based on applied force. Differences using the prescribed displacement method of contraction were usually limited to one-hundredths of a millimeter. The data shows that with a stiffer muscle and tendons there is a reduction in the force distribution over the model. This stiffer soft-tissue acted as a damper and lessened the amount of force placed on the muscle/tendon interfaces. When the material properties for the muscle and tendon were looser or softer, there was an overall increase in movement in X, Y, and Z for the applied force method of contraction and an increase in the von Mises stress along the muscle/tendon interfaces. The amount of displacement for prescribed displacement was limited to hundredths of a millimeter while the amount of displacement from applied force varied to millimeters to tenths of millimeters difference. The most dramatic difference was in the uniform reduction or increase in von Mises stress. Stiffer materials reflected a reduction in stress while softer materials reflected an increase. The disparity in displacement between applied force and prescribed displacement is not too surprising. The soft-tissue shortens in relationship to the material properties stiffness and the force that is applied. The prescribed displacement method of contraction does not take that soft-tissues material properties into account. One concern for this experiment lies with the overall limited range the combined contraction of the muscles of the rotator cuff. Differences in displacement might be more evident on a joint with a larger range of motion. Future studies should examine this possibility.

For the injury experiment, there was a reduction in the number of elements which had a foreseeable reduction in the simulation solve time. The applied force method of contraction resulted in greater movement in X and Y but lesser in Z with the difference being within tenths of a millimeter. The von Mises stress increased for the applied force. These results infer that with the reduced number of splines, there is a reduction in the number of antagonistic force vectors which allowed for greater movement and an increase in the stress placed on the muscle/tendon interfaces. For the prescribed displacement, there was a decrease in the amount of displacement in X, Y and Z in millimeters and tenths of millimeters. This reduction in movement also coincided with a decrease in von Mises stress. This pattern infers that when using a ridged guideline of 50% reduction in spline length to mimic muscle contraction, any loss of splines contributes to additional loss of movement.

For both Phase II and Phase III, the consistency of the average about of displacement in the X, Y and Z coordinates implies a high level of stability in the model. This may be on account of the inclusion the sphere as a rigid body for the center of rotation. Furthermore, one of the chief purposes of muscles of the rotator cuff is to keep the shoulder stable. Both the sphere and the musculature may be working in conjunction here. A breakdown of the angular displacement would be of value here for further comparison and will be tested in future study.

The examination of what role material properties had on the model reflect that stiffer or softer materials will behave similarly when applied force is used as the method of

contraction. Prescribed displacement, not surprisingly, does not take material properties into account and is consistent to the one-hundredth of a millimeter. It is recommended that applied force be used as the method of contraction to allow for the important anatomical and physiological antagonistic relationship of muscles which the prescribed displacement method ignores.

The injury scenario presented a prime example of the important of spline placement and contraction method. When combined with applied force, the missing splines allowed for an increase in movement on account of the decrease in antagonistic aspects of the muscles. When combined with the prescribed displacement, there is an overall decrease in movement which shows how the presence or absence of splines reduces the displacement in X, Y and Z. Future studies will examine if these relationships continue on musculoskeletal joint combinations that have a greater range of motion.

CHAPTER 4:

DISCUSSION AND CONCLUSIONS

The purpose of this project was to examine how different levels of simplification and representation of muscle geometry can affect the performance of a finite element anatomical model using a commercially available finite element analysis (FEA) software package (*COMSOL*). This was examined by utilizing three different geometric muscle representations in conjunction with the Hill mathematical model and linear elastic material properties. The three different representations of muscle included a bulk, central line of action (CLOA) and spline model. The study was conducted in a series of phases. Phase I was a pilot study examining how the different 3-D representations of skeletal muscle behaved while being limited to simple geometric shapes. Upon completion of Phase I, Phase II and Phase III replaced the simple geometry with increasing complex anatomical meshes. FEA solve time and results for the three different scenarios were compared. It was the hypothesis of this study that the bulk, CLOA and spline representations of skeletal muscle, combined with linear elastic properties, would have statistically similar results for finite element simulation of muscle contraction.

Phase I

Phase I successfully modeled and solved simplistic representations of skeletal muscle contractions within commercially available software. The calculations for force and force vectors as well as the linear elastic material properties were uniform across the scenarios. The data concerning element count and solve time performed as expected with the greater element counts correlating with longer solve times. However, for these mathematical geometries, even with the most complex geometry of the spline model, the time needed to solve the analysis was relatively short. These solve times were anticipated to increase in Phases II and III as the model complexity increased.

An average displacement of Phase I was 63.49 mm and fell within the range of the 60 mm – 70mm expected from the maximum contraction of a 200 mm muscle.[62] This model was in a straight line along the x-axis and there were no joint mechanics involved. For each scenario, the von Mises stress displayed that the tendon acted as a damper in force transmission from muscle to bone as anticipated.[62] The von Mises stress appears relatively stable as well with a 95% confidence interval of 39.71 N/cm^2 – 41.43 N/cm^2 but there was an upward trend as the diameters of the muscle geometries narrowed. This trend may be on account of the greater relative deformation of the narrower muscle representation. The relative uniformity of the displacement and von Mises stress suggest that the different 3-D representations of muscle geometry are able to capture similar phenomena. These initial findings suggest that 3-D muscle representation, be it a bulk, CLOA or spline, may be equally valid when simulating

displacement and von Mises stress distribution, and therefore human motion as well. The ultimate displacement and deformation of the moving bone was strikingly similar. It remained to be seen if the jump from primitive geometric shapes to biologically created geometries would have rendered similar results.

Phase II and Phase III

In Phase II and Phase III, the level of complexity was increased with the simple mathematical geometry being replaced by the anatomical geometries of a human shoulder joint. The modeling of anatomical structures was based around the Visible Human Male dataset and the reconstruction of 3-D volumes from serially sectioned image data. The model construction and mesh creation resulted in higher element counts than those found in Phase I. The data concerning element count and its associated increase with the addition of larger and more complex geometries is not surprising. However, the default error threshold of COMSOL prevented convergence of a solution. When these error safeguards were removed, the resulting values for displacement and von Mises stress were well beyond anything anatomically possible.

Troubleshooting efforts involved checking and rechecking the mathematical calculations, checking the model scales as well as the units for each numerical value. No errors in this regard were found. The musculotendon parameters of volume, PCSA, Fmax were all compared against known applications of the VHM dataset and were comparable.[70] Any potential differences may be on account that Garner et al used

images at 5 mm slice increments, while this study used the full 1 mm slice increments.[70] Furthermore, since many calculations are a result from the same optimal fiber length values from literature, the difference in volumes would account for the difference in the resulting PCSA and Fmax values. The differences between the musculoskeletal parameters were statistically insignificant.

It is our conclusion is that the use of a linear elastic model may be the source of the error. Personal Communication with COMSOL suggested that a hyperelastic model maybe a better option for this particular set of geometries. The strain value being above 10% is one indication and a potential source of a lack of convergence. Furthermore, it is possible that the more complex anatomical geometries themselves are creating singularities of very high values and not allowing for the model to converge.[74] However, the use of a linear elastic model should still work under the circumstances of this study since the forces involved do not extend into the plasticity range.[75]

Due to the inability to solve the simulation for either Phase II or Phase III, adjustments had to be made. The added complexity of joint mechanics required the additional control of a center of rotation with in the humeral head. A rigid sphere was created at the center of the humeral head to serve as a center of rotation. Furthermore, in addition to the Fmax simulation of muscle contraction, a prescribed displacement method was also used for the bulk, CLOA and spline muscle representations for Phase II and Phase III. Additional experiments were conducted examining the role of material properties as well as a simulated shoulder cuff injury.

For Phase II and III, with an uninjured representation of anatomy and standard material properties, the amount of variation in the displacement was very low for both scenarios when broken down to their X,Y,Z components. For the Prescribed Displacement scenario, the average X, Y and Z was 0.82 ± 0.17 mm, 1.71 ± 1.39 mm and 0.11 ± 0.05 mm respectively for Phase II and 1.58 ± 1.37 mm, 1.23 ± 0.5 mm and 0.32 ± 0.27 mm respectively for Phase III. For the Applied Fmax scenario, the average X, Y and Z was 1.3 ± 0.44 mm, 1.62 ± 0.87 mm and 0.22 ± 0.19 mm respectively for Phase II and 1.58 ± 1.37 mm, 1.23 ± 0.5 mm and 0.32 ± 0.27 mm respectively for Phase III.

For the experiment with variable material properties, the relationship between applied force and the soft tissue rose to the forefront. The stiffer scenario, when combined with the applied force method of contraction, had an average decrease of displacement in X, Yt and Z of -1.08 ± 1.16 mm, -0.41 ± 0.41 mm and -0.12 ± 0.1 mm respectively. The less stiff scenario, when combined with the applied force method of contraction, had an average increase of displacement in X, Y and Z of 0.65 ± 0.74 mm, 0.61 ± 0.18 mm and 0.78 ± 0.15 mm respectively. The average difference in movement was limited to hundredths or thousandths of a millimeter when either the stiffer or softer materials were combined with the prescribed displacement. The stiffer scenario had an average difference of movement in X, Y and Z of -0.023 ± 0.09 mm, 0.1 ± 0.13 mm and 0.01 ± 0.06 mm respectively. The softer scenario had an average difference of movement in X, Y and Z of -0.0067 ± 0.06 mm, 0.12 ± 0.16 mm and 0.02 ± 0.052 mm respectively. The von Mises stress followed a typical pattern where the softer materials had an increase in stress levels, while the stiffer materials had a decrease in stress levels.[80,81] The fact that

the prescribed displacement method of contraction did not take the material properties into account in regards to affecting the movement suggests that the applied force if more representative of an anatomical contraction. Furthermore, the applied force also allows the muscles to maintain their antagonistic or synergistic relationships which the prescribed displacement does not. These findings should be explored further to see if these results hold true for a joint with a greater range of motion.

The injury scenario served as an example of how the 3-D spline representation can be used to mimic partial muscle tears. The missing splines, when combined with the applied force contraction, displayed how their absence allowed the resulting motion to increase in X and Y but decrease in Z. The reduced number of splines created a reduction in the number of antagonistic interactions and allowed for the greater movement. The prescribed displacement contraction for the injury scenario had the opposite effect and decreased the overall movement. Again, these findings should be explored further under a greater range of motion.

Future directions will include substituting the linear elastic model with a hyperelastic or viscoelastic one. Other studies have attempted this to varying levels of success.[51,57,63,76] The hyperelastic and viscoelastic models should be compared against one another. Additionally, efforts will be made to find alternative ways to utilize the linear elastic models and see if comparison against the hyperelastic and viscoelastic models are possible. Furthermore, this study focuses on muscles undergoing active contraction.

Future directions would also include testing if the linear elastic model would be better suited for passive muscle interaction.

It should also be mentioned that joints are not just muscles and bone, but include ligaments, synovial fluid, articular cartilage and so on. All these anatomical structures contribute to the natural center of rotation for a given joint. It would be of benefit to compare an artificial center of rotation (like the internal sphere) to a more complex anatomical model that relied on the other supportive tissues of the joint.

The goal of this study was to use commercially available FEA software to compare the different geometric representations (bulk, CLOA and spline) of human skeletal muscle and the effect these representations had on muscle contraction. For Phase I, the results supported the hypothesis which showed that a linear elastic model when combined with a primitive set of geometries resulted in similar results across the bulk, CLOA and spline scenarios. After constructing a center of rotation for the shoulder joint, Phase II and Phase III suggests that the introduction of biological geometries, combined with the linear elastic model for skeletal muscle further supports this hypothesis.

The overall uniformity suggests a large amount of stability in the shoulder joint. However, this may be a result of the artificially constructed center of rotation. The CLOA had the shortest solve time which is not surprising due to it being the simplest model. The fact that it solved faster by an hour to several hours versus the Bulk and Spline scenarios implies its usefulness to joint movement studies. CLOA muscle

representation would be of great use in studies such as gait analysis and kinematic simulation.[81] That being said each 3-D representation has its own advantages and disadvantages depending on what is being simulated. The bulk and spline representations would have a greater use in injury simulation and analysis.[82] Bulk muscle representation would lend itself to scenarios of direct muscle impact analysis or compression analysis and the affect it has on a muscle's ability to contract.[73,83] Bulk modeling would also lend itself to modeling partial tears by removing aspects of the tendon/bone interface and see how it affects force transmission. Spline modeling, like in the injury analysis in this study, could also be used to model partial tears as well while. Furthermore, spline modeling would be a representative way of examining muscle fiber behavior under contraction.[50,84]

In conclusion, this study suggests that muscle behavior is stable regardless of 3-D geometric representation. The experiment in material property variability infers that the applied force method of contraction is preferred to the prescribed displacement contraction method in that it allows for a more antagonistic and synergistic relationship between muscle forces. The results from the injury experiment further supports this idea while also providing an example of a practical application. This information is important for engineers or anyone who researches joint biomechanics such as orthopedics, who can now with confidence use 3 different representations of muscle models interchangeable for their experimental analyses. In research and development, both in industry and in academia, time versus cost while maintaining high level accuracy is a primary concern. The results from this study show that researchers can now use a time-

efficient model without concern of drastically reducing the quality of their muscle analyses. Which model just depends on what aspect of musculoskeletal mechanics, such as movement or injury simulation, they want to simulate.

REFERENCES

(1)   Ciobanu O (2006) The Use of Computer Aided Design (CAD) Environment in 3-D Reconstruction of Anatomic Surfaces. *Medicine Meets Virtual Reality 14.* J.D. Westwood et al. (Eds.) IOC Press: 102 -104.

(2)   Brekelmans WA, Poort HW and TJ Sloof. A New Method to Analyse the Mechanical Behavior of Skeletal Parts. Acta Orthopaedica, 1972, 43(5):301-317.

(3)   Godest AC, Beaugonin M, Haug E, Taylor M, and PJ Gregson. Simulation of a knee joint replacement during a gait cycle using explicit finite element analysis. Journal of Biomechanics. 2002, 25(2):267-275.

(4)   Helwig P, Faust G, Hindenlang U, Kröplin B, and C Eingartner. Finite Element Analysis of a Bone-Implant System with the Proximal Femur Nail. Technology and Healthcare, 2006, 14:411-419.

(5)   Cilingir AC, Ucar V and K Recep. Three-Dimensional Anatomic Finite Element Modeling of Hemi-Arthroplasty of Human Hip Joint. Trends in Biomaterials & Artificial Organs. 2007, 21(1):63-72.

(6)   Delp SL, Ringwelski DA and NC Carroll. Transfer of the rectus femoris: Effects of transfer site on moment arms about the knee and hip. Journal of Biomechanics, 1994, 27(10):1201-1211.

(7)   Hoy MG, Zajac FE and ME Gordon. A musculoskeletal model of the human lower extremity: The effect of muscle, tendon, and moment arm on the moment-angle relationship of musculotendon actuators at the hip, knee and ankle. Journal of Biomechanics, 1990, 23(2):157-169

(8)   Chao EYS, Lynch JD and MJ Vanderploeg. Simulation and animation of musculoskeletal joint system. Journal of Biomechanical Engineering. 1993, 115:562-568.

(9)   Gu YD, Ren XJ, Li JS, Lake MJ, Zhang QY and YJ Zeng. Computer Simulation of Stress Distribution in the Metatarsals as Different Inversion Landing Angles Using the Finite Element Method. International Orthopaedics. 2010, 34(5):669-676.

(10)   Arab-Ghanbari M, Khani MM, Arefmanesh A, and F Tabatabai-Ghomshe. Analysis of Blood Turbulent Flow in Carotid Artery Including the Effects of Mural Thrombosis Using Finite Element Modeling. American Journal of Applied Sciences. 2009, 6(1):337-345.

(11)   Khani MM, Shadpour MT, Delavarpour S, Naghizadeh S and A Avolio. Dynamic Stress Analysis of the Arterial Wall Utilizing Physiological Pressure Waveforms. American Journal of Applied Sciences. 2008, 5:1285-1291.

(12)   Zhai J and G Narwani. Development of a Human Body Finite Element Model for Restraint System R&D Applications. Proceedings 19th International Technical Conference on the Enhanced Safety of Vehicles. 2005. Washington DC.

(13)   Ganpule S, Alai A, Plougonven E and N Chandra. Mechanics of Blast Loading on the Head Models in the Study of Traumatic Brain Injury Using Experimental and Computational Approaches. Biomechanics and Modeling in Mechanobiology. 2013, 12:511-531.

(14)   Van Donkelaar CC, Willems PJB, Muijtens AMM and MR Drost. Skeletal Muscle Transverse Strain During Isometric Contraction at Different Lengths. Journal of Biomechanics. 1999, 32:755-762.

(15)   Loerakker S, Stekelenburg A, Strijkers GJ, Rijpkema JM, Baaijens FPT, Bader DL, Nicolay K and CWJ Oomens. Temporal Effects of Mechanical Loading on Deformation-Induced Damage in Skeletal Muscle Tissue. Annals of Biomedical Engineering. 2010, 38(8):2577-2587.

(16)   Teran J, Sifakis E, Blemker S, Ng-Thow-Hing V, Lau C and R Fedkiw. Creating and Simulating Skeletal Muscle from the Visible Human Data Set. IEEE Transactions on Visualization and Computer Graphics, Vol 11, 2005 3:317-328.

(17)   Blemker SS and SL Delp. Three-Dimensional Representation of Complex Muscle Architectures and Geometries. Annals of Biomedical Engineering, 2005, 33(5):661-673.

(18)   Lee D, Ravichandiran K, Jackson K, Fiume E and A Agur. Robust estimation of physiological cross-sectional area and geometric reconstruction for human skeletal muscle. Journal of Biomechanics. 2012, 45(8):1507-1513.

(19)   Hill AV. The heat of shortening and the dynamic constants of muscle. Proceedings of the Royal Society London B. 1938, 126:136-195.

(20)   Huxley AL. Muscle structure and theories of contraction. Progress in Biophysics and Biophysical Chemistry. 1957, 7:255-318.

(21) Winters JM and SLY Woo. Multiple Muscle Systems: Biomechanics and Movement Organization. Springer-Verlag. New York, NY. 1990.

(22) Nigg BM and W Herzog. Biomechanics of Musculo-skeletal System. 3rd Ed. Wiley. Chichester, UK. 2006.

(23) Fung YC. Biomechanics: Mechanical Properties of Living Tissues. Springer. New York 1993.

(24) Lieber RL. Skeletal Muscle Structure, Function, and Plasticity: The Physiological Basis of Rehabilitation. 2nd Ed. Lippincott Williams & Wilkins. Philadelphia, PA 2002.

(25) Moore KL, Augr AMR and AF Dalley. Essential Clinical Anatomy, 4th Ed. Lippincott Williams & Wilkins. Philadelphia, PA 2011.

(26) Anderson DL. Role of rapid prototyping in preoperative planning and patient-specific implant generation. IEEE Eng. Medicine and Biol. Pp. 558-559, Jan 1996.

(27) Lee TY, Sun YN, Lin YC, Lin L, and C Lee. Three-dimensional facial model reconstruction and plastic surgery simulation. IEEE Transactions on Information Technology in Biomedicine, 1999, 3(3):214-220.

(28) Spitzer V, Ackerman MJ, Scherzinger AL and D Whitlock. The Visible Human Male: A Technical Report, JAMIA 1996, 3:118-130.

(29) Park JS, Chung MS, Hwang SB, Shin BS, and HS Park. Visible Korean Human: its Techniques and Applications. Clinical Anatomy. 2006 3:216-225.

(30) Zhang SX, Heng PA, Liu ZJ. Chinese Visible Human Project. Clinical Anatomy. 2006, 19:204-215.

(31) Bai X, Wei G, Ye M, Wang D, Hu Y, Liu Z, Nie W, Zhang L, Ji W, Li Y and C Wang. Finite Element Musculoskeletal Modeling of Mechanical Virtual Human of China. The 2nd International Conference on Bioinformatics and Biomedical Engineering, Shanghai, 2008

(32) Clough R. The Finite Element in Plane Stress Analysis. Proc. 2nd ASCE Conf. on Electronic Computation. Pittsburgh, Pa., Sept. 1960.

(33) Zienkiewicz O and R Taylor. The Finite Element Method Volume 1: The Basis. Oxford: Butterworth-Heinemann, 2000.

(34) Liu G and S Quek. The Finite Element Method A Practical Course. Oxford: Butterworth-Heinemann, 2003.

(35)   Logan DL. A First Course in the Finite Element Method. 5th Ed. CL Engineering, 2011.

(36)   Bayraktar HH, Morgan EF, Niebur GL, Morris GE, Wong EK and TM Keaveny. Comparison of the elastic and yield properties of human and cortical bone tissue. Journal of Biomechanics. 2004, 37:27-35

(37)   Hofmann T, Heyroth F, Meinhard H, Fränzel W and K Raum. Assessment of composition and anisotropic elastic properties of secondary osteon lamellae. Journal of Biomechanics. 2006, 39:2282-2294.

(38)   Kaneko TS, Bell JS, Pejcic MR, Tehranzadeh J and JH Keyak. Mechanical properties density and quantitative CT scan data of trabecular bone with and without metastases. Journal of Biomechanics. 2004, 37:523-530.

(39)   Staubli HU, Schatzmann L, Brunner P, Ricón L and P Nolte. Mechanical tensile properties of the quadriceps tendon and patellar ligament in young adults. The American Journal of Sports Medicine. 1999, 27:27-34.

(40)   Rotter N, Tobias G, Lebi M, Roy AK, Hansen MC, Vacanti CA and LI Bonassar. Age-related changes in the composition and mechanical properties of human nasal cartilage. Archives of Biochemistry and Biophysics, 2002, 403:132-140.

(41)   COMSOL (Version 4.3b) [Computer Software]. Stockholm, Sweden: COMSOL. Retrieved August 9, 2013. Available from http://www.comsol.com

(42)   ANSYS (Version 14.0) [Computer Software]. Canonsburg, PA: Ansys, Inc. Retrieved July 9, 2012. Available from http://ansys.com

(43)   Abaqus (Version 6.11) [Computer Software]. Paris, France: Dassault Systemes S.A. Retrieved July 9, 2012. Available from http://www.simula.com

(44)   Ford, JM. The Virtual Hip: An Anatomically Accurate Finite Element Model Based on the Visible Human Dataset. Master's Thesis. University of South Florida. Department of Chemical and Biomedical Engineering. 2010.

(45)   Fernandez JW, Mithraratne P, Thrupp SF, Tawahi MH and PJ Hunder. Anatomically based geometric modeling of the musculo-skeletal system and other organs. Biomechanics and Modeling in Mechanobiology, 2003, 2:139-155.

(46)   SIMM. [Computer Software] Santa Rosa, CA. Musculographics Inc. SIMM. Retrieved July 9, 2012. Available from http://musculographics.com/products/simm.html

(47)   LifeModeler. [Computer Software] San Clemente, CA. LifeModeler, Inc. Retrieved July 9, 2012. Available from https://www.lifemodeler.com/

(48)   AnyBody. [Computer Software] Aalborg, Denmark. AnybodyTechnology, A.S..
        September 29, 2011. Available from http://www.anybodytech.com/

(49)   Delp SL, and JP Loan. A Computational framework for simulating and analyzing
        human and animal movement. IEEE Computing in Science and Engineering.
        2000, 2(5):46-55.

(50)   Rehorn MR and SS Blemker. The effects of aponeurosis geometry on strain
        injury susceptibility explored with a 3-D muscle model. Journal of Biomechanics.
        2010, 43:2574-2581

(51)   Martins JAC, Pires EB, Salvado R and PB Dinis. A Numerical Model of Passive
        and Active Behavior of Skeletal Muscle. Computer Methods in Applied
        Mechanics and Engineering. 1998, 151:419-433.

(52)   Gans C. Fiber architecture and muscle function. Exercise & Sports Science
        Reviews, 1982, 10:160-207

(53)   Alexander AV. The dimension of knee and ankle muscles and the forces they
        exert. Journal of Human movement Studies. 1975, 1:115-123.

(54)   Asakawa DS, Pappas Gp, Blemker SS, Drace JE and SL Delp. Cine phase-
        contrast magnetic resonance imaging as a tool for quantification of skeletal
        muscle motion. Seminars in musculoskeletal radiology. 2003, 7(4): 287-295

(55)   Shue GH and PE Crago, Muscle–tendon model with length history-dependent
        activation-velocity coupling, Annals Biomed. Eng. 1998, 26:369–380.

(56)   Gareis H, Solomonow M, Baratta R, Best R and R D'Ambrosia, The isometric
        length–force models of nine different skeletal muscles, J. Biomechanics, 1992,
        25:903–916.

(57)   Johansson T, Meier P and R Blickhan, A finite-element model for the mechanical
        analysis of skeletal muscles, J. Theor. Biol. 2000, 206:131-149.

(58)   Shue GH and PE Crago, Muscle–tendon model with length history-dependent
        activation-velocity coupling, Annals Biomed. Eng. 1998, 26:369–380.

(59)   Ward SR, Eng CM, Smallwood LH and RL Lieber. Are Current Measurements of
        Lower Extremity Muscle Architecture Accurate? Clinical Orthop Relate Res,
        2009, 467:1074-1082.

(60)   Bangash MYH, Al-Obaid YF, Bangash FN and T Bangash. Trauma An
        Engineering Analysis with Medical Case Studies Investigation. Springer. New
        York, NY. 2007

(61) Lewis G and KM Shaw. Modeling the tensile behavior of the human Achilles tendon. Bio-Medical Materials and Engineering. 1997, 7(4):231-244.

(62) Marieb, EN and K Hoehn. Human Anatomy & Physiology. Pearson. Upper Saddle River, NJ. 2012.

(63) Tsui CP, Tang CY, Leung CP, Cheng KW, Ng YF, Chow DH and CK Li. Active finite element analysis of skeletal muscle-tendon complex during isometric, shortening and lengthening contraction. Bio-Medical Materials and Engineering. 2004, 14:271-279.

(64) Mendes, S. Development of an Improved Finite Element Muscle Model and the Investigation of the Pre-Loading Effects of Active Muscle on the Femur During Frontal Crashes. Master's Thesis. Worcester Polytechnic Institute. Department of Civil Engineering. 2010.

(65) Martini FH, Nath JL and EF Bartholomew. Fundamentals of Anatomy and Physiology. 9th Ed. Benjamin Cummings. San Francisco, CA. 2011.

(66) Jenkins DB. Hollinshead's Functional Anatomy of the Limbs and Back. 9th Ed. Saunders. Philadelphia, PA. 2008.

(67) Sherwood L. Human Physiology: From Cells to Systems. 8th Ed. Cengage Learning. Independence, KY. 2012.

(68) Curtis AS, Burbank KM, Tierney JJ, Scheller AD and AR Curran. The Insertional Footprint of the Rotator Cuff: An Anatomic Study. Arthroscopy: The Journal of Arthroscopic and Related Surgery. 2006, 22(6)603-609.

(69) Mochizuki T, Sugaya H, Uomizu M, Maeda K, Matsuki K, Sekiya I, Muneta T and K Akita. Humeral insertion of the supraspinatus and infraspinatus. New anatomical findings regarding the footprint of the rotator cuff. The Journal of Bone and Joint Surgery. 2008, 90:962-969.

(70) Garner BA and MG Pandy. Musculoskeletal Model of the Upper Limb Based on the Visible Human Male Dataset. Computer Methods in Biomechanics and Biomedical Engineering, 2001, 4:93-126.

(71) Lieber RL, Jacobson MD, Fazeli BM, Abrams RA and MJ Botte. Architecture of selected muscles of the arm and forearm: Anatomy and implications for tendon transfer. Journal of Hand Surgery, 1992, 17A, 787-798.

(72) Winters JM and L Stark. Estimated mechanical properties of synergistic muscles involved in movements of a variety of human joints. Journal of Biomechanics. 1988, 21:1027-1041

(73) Mendes S. Development of an Improved Finite Element Muscle Model and the Investigation of the Pre-Loading Effects of Active Muscle on the Femur During Frontal Crashes. Master's Thesis. Worcester Polytechnic Institute. Department of Civil Engineering. 2010.

(74) Kumar, C. COMSOL Applications. (2013, May 3). Email.

(75) Bronzino, JD et al. Introduction to Biomedical Engineering. Academic Press. Waltham. MA. 2005.

(76) Teran J, Blemker SS, Ng Thow Hing V, and R Fedkiw. Finite Volume Method for the Simulation of Skeletal Muscle. Proceedings of the 2003 ACM SIGGRAPH/Eurographics symposium on Computer Animation. 2003:68-74.

(77) Lu YT, Zhu HX, Richmond S and J Middleton. A visco-hyperelastic Model for Skeletal Muscle Tissue Under High Strain Rates. Journal of Biomechanics, 2010, 43:2629-2632.

(78) Tang CY, Zhang G and CP Tsui. A 3D Skeletal Muscle Model Coupled with Active Contraction of Muscle Fibers and Hyperelastic Behaviour. Journal of Biomechanics, 2009, 42:865-872.

(79) Shim JS and DC Watts. An Examination of the Stress Distribution in a Soft-Lined Acrylic Resin Mandibular Complete Denture by Finite Element Analysis. The International Journal of Prothodontics, 2000, 13(1):19-24.

(80) Hammond AS, Dumont ER, and RC McCarthy. The Effect of Unerupted Permanent Tooth Crowns on the Distribution of Masticatory Stress in Children. Plos One, 2011, 6(12):1-6.

(81) Erdemir A, McLean S, Herzog W and AJ van den Bogert. Model-basted estimation of muscle forces exerted during movements. Clinical Biomechanics, 2007, 22(2):131-154.

(82) Büchler P, Ramaniraka NA, Rakotomanana LR, Iannotti JP, and A Farron. A finite element model of the shoulder: application to the comparison of normal and osteoarthritic joints. Clinical Biomechanics, 2002, 17(9-10):630-639.

(83) Linder-Ganz E, Shabshin N, Yacov I, and A Gefen. Assessment of mechanical conditions in sub-dermal tissues during sitting: A combined experimental-MRI and finite element approach. Journal of Biomechanics, 2006, 40(7):1443-1454.

(84) Blemker SS, Pinsky PM, and SL Delp. A 3D model of muscle reveals the causes of nonuniform strains in the biceps brachii. Journal of Biomechanics, 2005, 38(4): 657-665.

(85)   Lieber RL and J Fridén. Clinical Significant of Skeletal Muscle Architecture. Clinical Orthopaedics and Related Research, 2001, 383:140-151

(86)   Spitzer, VM and DG Whitlock. Atlas of the Visible Human Male. Jones and Bartlett, Sudbury, MA. 1998.

(87)   Wood JE, Meek SG and SC Jacobsen. Quantitation of Human Shoulder Anatomy for Prosthetic Arm Control – II. Anatomy Matrices. Journal of Biomechanics, 1989, 22:309-325.

(88)   Peterson SL and GM Rayan. Shoulder and Upper Arm Muscle Architecture. Journal of Hand Surgery, 2011, 36A:881-889.

(89)   Ward SR, Hentzen ER, Smallwood LH, Eastlack RK, Burns KA, Fithian DC, Friden J, and RL Lieber. Rotator Cuff Muscle Architecture. Clinical Orthopaedics and Related Research, 2006, 448:157-163.

(90)   Keating JF, Waterworth P, Shaw-Dunn J and J Crossan. The Relative Strengths of the Rotator Cuff Muscles: A Cadaver Study. Journal of Bone and Joint Surgery, 1993, 75:137-140.

(91)   Tingart MJ, Apreleva M, Lehtinen JT, Capell B, Palmer WE, and JJ Warner. Magnetic Resonance Imaging in Quantitative Analysis of Rotator Cuff Muscle Volume. Clinical Orthopaedics and Related Research, 2003, 415:104-110.

(92)   Zanetti M, Gerber C and L Hodler. Quantitative Assessment of the Muscles of the Rotator Cuff with Magnetic Resonance Imaging. Investigative Radiology, 1998, 33(3):163-170.

(93)   Lehtinen JT, Tingart MJ, Apreleva M, Zurakowski D, Palmer W and JJ Warner. Practical Assessment of Rotator Cuff Muscle volumes Using Shoulder MRI. Acta Orthopaedica Scandinavica, 2003, 74(6):722-729.

(94)   Ackerman MJ, Yoo T, and D Jenkins. From Data to Knowledge – the Visible Human Project Continues. Studies in Health Technologies and Informatics, 2001, 84:887-890.

APPENDICES

Appendix A:

Rotator Cuff Muscle Volume

A.1 Abstract

Skeletal muscle architectural properties plays a critical role in the calculation of the potential behavior of individual muscles. Characteristics such as volume, physiological cross-sectional area (PCSA), optimal fiber length and muscle pennation angle all play a significant part in the calculation of how much force a muscle can generate. Furthermore, muscle architectural properties influence one another. A comparison was made with the Visible Human Male's (VHM) rotator cuff muscles of this study, with other studies that utilized the VHM as well as studies that measured muscle architecture in both cadavers and living people.

A.2 Introduction

Skeletal muscle architecture directly influences how a muscle behaves. The amount of force a muscle can generate, the influence fiber direction has on force generation, the amount of excursion possible, the speed of contraction can all be determined by muscle architecture. Muscle size and strength varies from person to person so differences are to be expected. However, certain architectural properties used in this study seemed slightly high and further examination was undertaken.

Appendix A Continued

Due to its role in the calculation of PCSA, muscle volume was of chief concern in this study. Muscle PCSA multiplied by the muscles specific tension constant directly determines the potential maximum force (Fmax) a muscle can generate. However, there is an accepted range of muscle specific tension PCSA is calculated by taking the total volume of a muscle and dividing it by the optimal muscle fiber length.[21,22,85] The muscle volumes of the VHM's supraspinatus, infraspinatus, teres minor and subscapularis used in this study were compared against several other studies that utilized the VHM as well as studies that measured muscle architecture in both cadavers and living people.

A.3 Materials and Methods

A.3.1 Data Set

The anatomy for this study was created based on the National Library of Medicine's (NLM) Visible Human Male (VHM) dataset from the Visible Human Project. The entire dataset is available for download upon request from the NLM's website. In total, the dataset consists of 1,878 slices as a tagged image file format (tiff) each with a resolution of 1760 x 1024. Each slice is 1 millimeter thick with a pixel size of 0.3528 millimeters. The slices are numbered in a fashion ranging from 1,001 to 2,878.[28,86] A segmented set of the VHM dataset was made available and utilized to facilitate the creation of 3D geometries. The initial segmentation was conducted by hand in Adobe's *Photoshop.*

Every structure segmented was assigned its own red, green and blue (RGB) value. This was a lengthy process that took a number of hands a considerable amount of time.

A.3.2 Models

The 3-D geometry was created via a multistep process within *Mimics* by Materialise. The images slices relevant to the scapula, humerus and the associated structures of the rotator cuff were imported into *Mimics*. This range began with image 1260 and extended through 1610 for a total of 351 images. The initial rough 3-D models of the supraspinatus, infraspinatus, teres minor and subscapularis, associated tendons and bones were created using the tessellation algorithm native to the software and exported as stereolithographs (STLs). Figure A.1 contains an example of some of the initial "rough" results from the segmented set.

Upon review, it was decided that an additional segmentation refinement step be conducted. An unsegmented VHM dataset was imported into *Mimics*. The STLs of the geometries of interest were imported into this file. Masks were generated from the imported geometries to use as a guide and a springboard to improve on the segmentation. The resulting masks segmentations were edited and new 3-D models were generated. Figure A.2 contains an example of the segmentation editing. This editing involved the removal or addition of pixels that belong to their respective

structures. These models, once again, were exported as STLs so they could be imported into 3-matics for remeshing and further mesh cleanup.
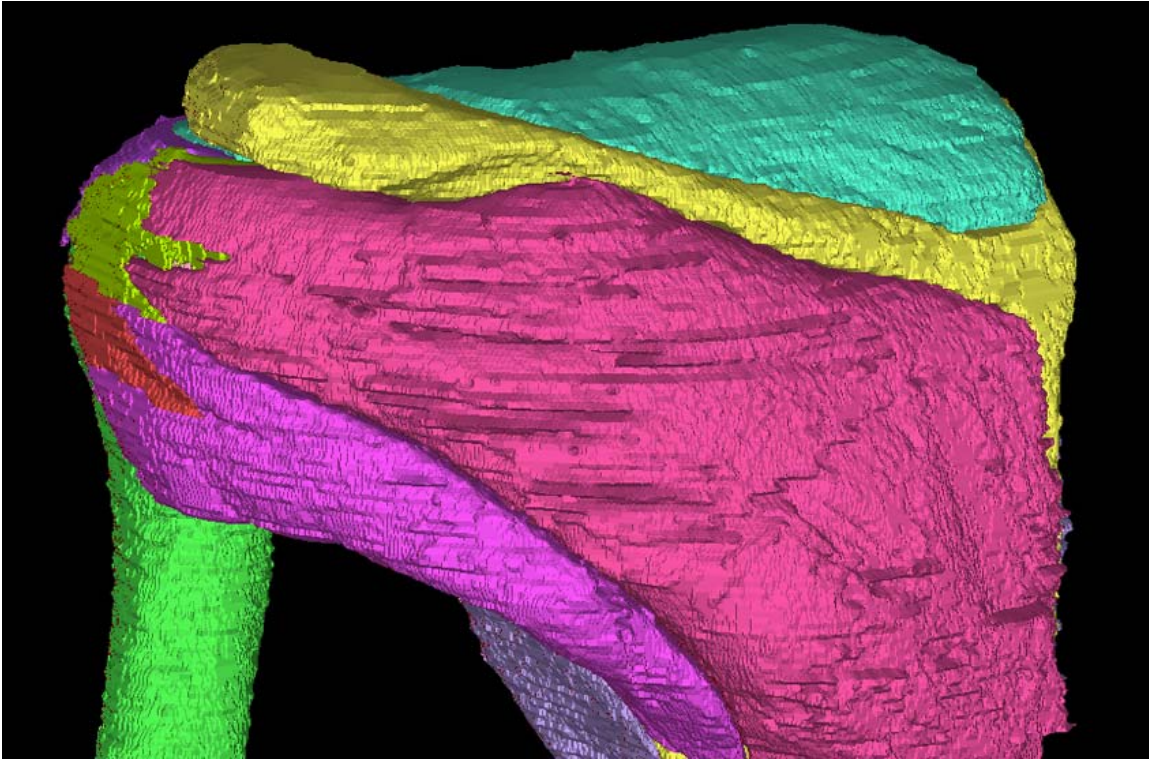

Figure A.1: Initial rough geometry.

Mesh clean up began with the wrapping of each geometry individually. This process closes any holes that may be present and makes a watertight mesh. Further cleanup involved the searching for and subsequent removal of any overlapping or intersecting triangles. The rotator cuff muscles and tendons were connected to the scapula and

humerus as a non-manifold mesh. Origin and insertion locations for each representative muscle was determined from personal knowledge, the VHM dataset as well as experimental results found in literature.[68,69] The muscle volumes were recorded for later comparison.
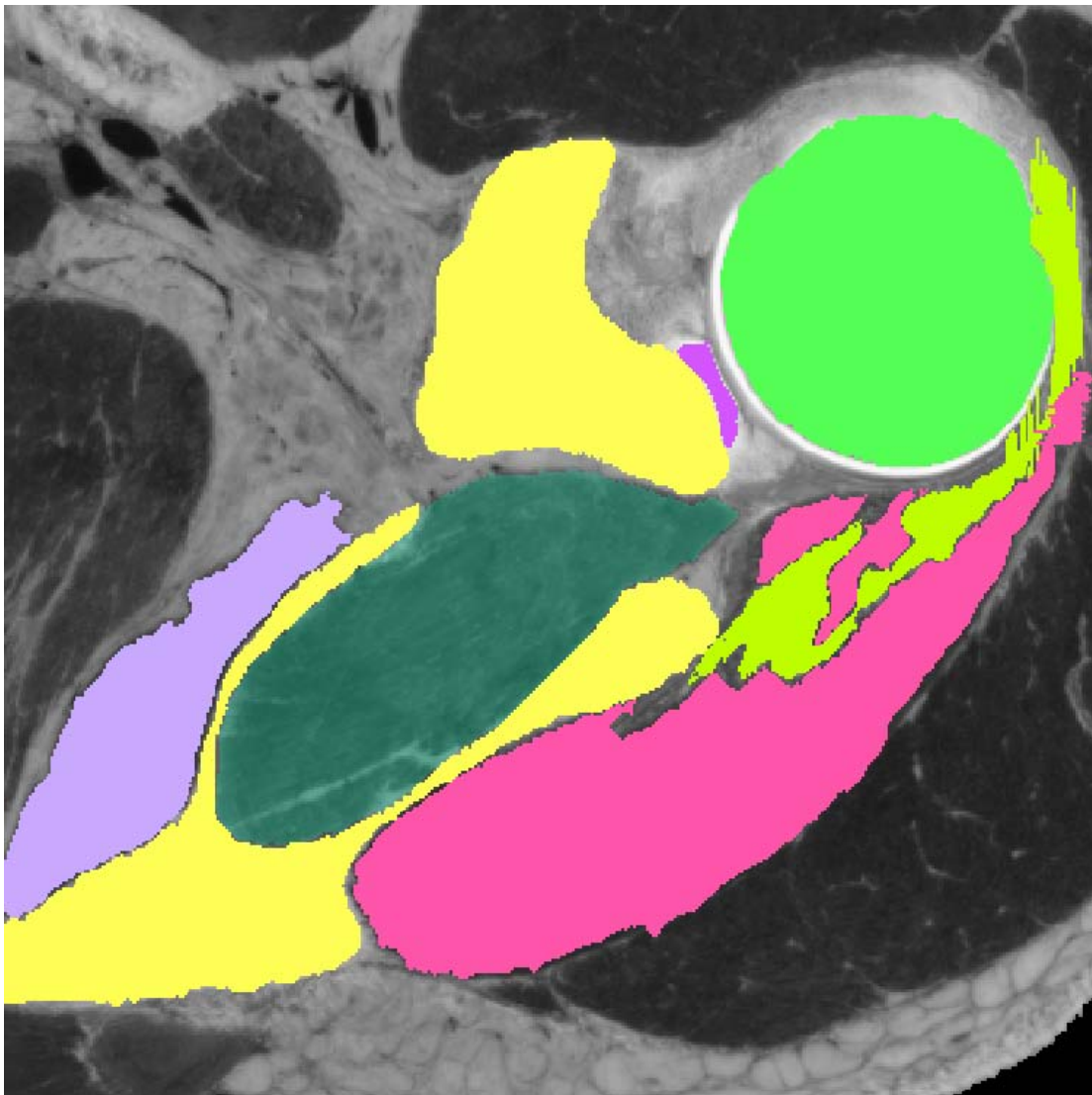

Figure A.2: Segmentation Mask Editing and Cleanup

Appendix A Continued

A.3.3 Dissection

A large adult donated male cadaver was selected as a source for comparison. The cadaver has been fixed by the Anatomical Board of the State of Florida. The left arm was skinned, and removed from the body. The scapula and the muscles of the rotator cuff was isolated and the overlying subcutaneous soft tissues was removed. Using sharp and blunt dissection the supraspinatus, infraspinatus, teres minor and subscapularis were removed from the bones. The tendons were cut from the muscles to isolate the muscle tissue.

The volume of the muscles was captured using water displacement. A 1000 ml graduate cylinder was filled to 600 ml. Each muscle was placed inside the graduated cylinder and the level of water displacement was recorded. The cylinder was cleaned and refilled between each measurement. The subscapularis needed to by bisected in order to fit inside the cylinder. The muscle volumes were recorded for later comparison.

A.3.4 Literature

Human upper limb architecture is of great interest of researchers of biomechanics, orthopedics and kinesiology. The rotator cuff receives a high level of academic scrutiny and the volumes, PCSA's and other muscle architectural properties have been recorded

in various journals and book chapters. These studies acquired their information from a variety of sources including cadaveric dissection[87-90] and medical imaging.[91-93] The subjects of these studies included both male and female individuals with a range of ages. Data from these studies was compiled for comparison against the muscle architecture of the VHM.

A.4 Results

The volumes acquired from the VHM modeling process, cadaveric dissection and literature review was compiled and compared. A representative image of the final muscle geometries can be seen in Figure A.3. The data of the supraspinatus, infraspinatus, teres minor and subscapularis can be seen in Table A.1.
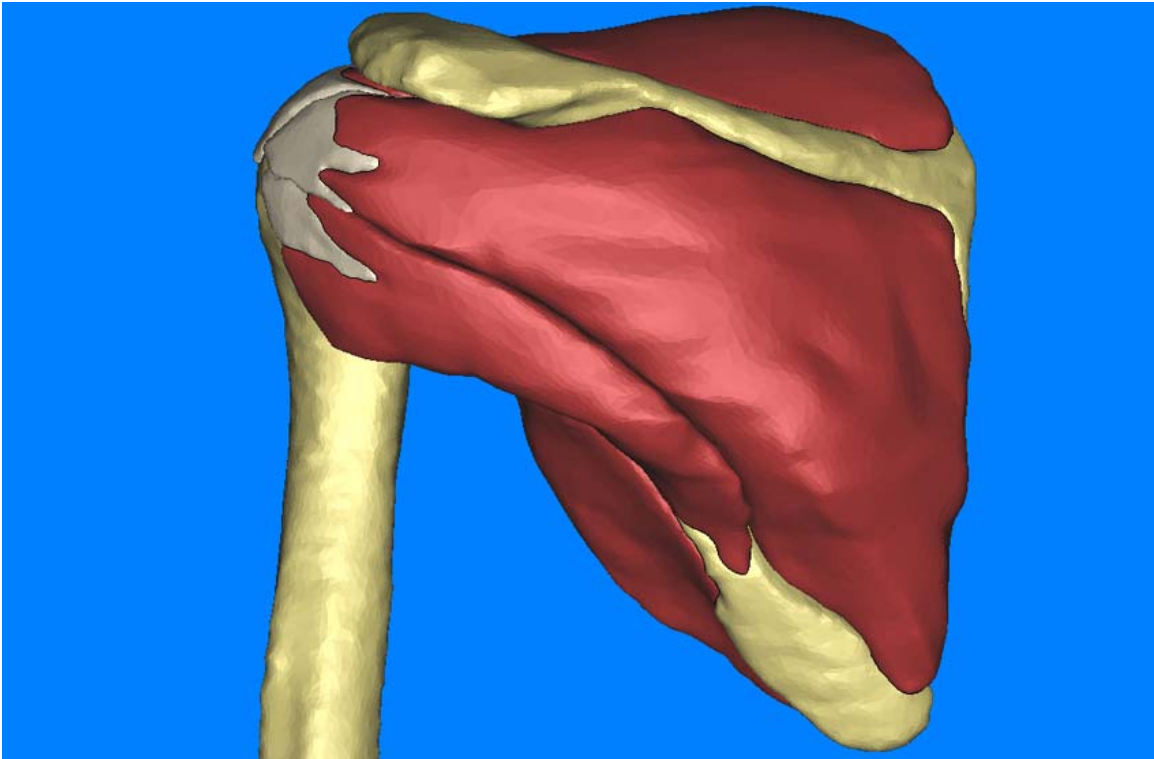
Figure A.3: Final Muscle Geometries

Appendix A Continued

Table A.1: VHM Muscle Numerical Volume Comparison

Muscle Name	This Study	Garner et al[70]	Cadaver Dissection	Peterson et al[88]	Wood et al[87]	Ward et al[89]	Keating et al[90]	Tingart et al[91]	Lehtinen et al[93]
Supraspinatus	88.23	89.23	55	31.68	39.33	35.9	23	36	36
Infraspinatus	225.01	225.36	175	80.256	85.21	82.4	44	-	-
Teres Minor	47.91	38.7	45	11.62	24.58	22.4	12.4	-	-
Subscapularis	262.24	318.52	220	-	121.26	107.5	53	99	99

Appendix A Continued

A.5 Discussion and Conclusions

The resulting VHM volumes for the supraspinatus, infraspinatus, teres minor and subscapularis was larger in all comparisons excluding the Garner et al study.[8] The range of the muscle volumes from the literature review for supraspinatus, infraspinatus, teres minor and subscapularis was $39.33 - 23$ cm^3, $85.21 - 44$ cm^3, $24.58 - 11.62$ cm^3, and $121.26-53$ cm^3 respectively. These are all well below both the VHM volumes from this study, the Garner et al study as well as the cadaver dissection study. The volumes from this study was closest to the Garner study with the volumes of the supraspinatus, infraspinatus, teres minor and subscapularis being within 1.13%, 0.16%, 19.22% and 21.46% respectively.

The cadaver study as well as the literature review displays the range and variability in muscle sizes from person to person. The majority of the data from the literature was from an elderly population, and often an equal mix of male and female subjects. This may account for the low average muscle volumes of these studies.[87-93] The larger volumes of the VHM may have been on account that the donor was a comparatively young and muscular man. It is possible that the donor for the VHM was naturally larger than elderly donors from literature. An additional aspect that may influence the volumes of the VHM musculature may lie in the freezing process involved in the creation of the VHM dataset. Freezing artifacts and embalming artifacts may have altered the soft

tissue. Other studies have expressed concerns regarding deformation, swelling and misalignment of images.[94]

The disparities between the VHM muscle volumes of this study and the Garner et al study may be on account of the differences in slice-thicknesses used in each study. This study utilized all the slices available, which allowed for a slice thickness of 1 mm. The Garner et al study used a slice thickness of 5 mm. The absence of all the available slices could account for the volume differences in the muscles, especially the teres minor and subscapularis.

Future studies should use medical imaging to capture muscle volumes and architectural properties from a wide range of ages and body types. Cadaveric studies are more often than not based on an elderly population. Medical imaging, be it magnetic resonance imaging or computed tomography would provide an in vivo dataset without the age limitations of cadaver studies.

ABOUT THE AUTHOR

Jonathan M. Ford was born in Las Vegas, Nevada and earned a dual baccalaureate with honors in English and History from the University of Nevada, Las Vegas. In 2009, he earned his Master's of Science in Medical Science (Anatomy) from the University of South Florida (USF) College of Medicine. In 2010, he earned his Master's of Science in Biomedical Engineering from the University of South Florida. He began pursuing his doctorate while working as a teaching assistant and researcher in the Department of Pathology and Cell Biology in the USF College of Medicine.

His time at USF has allowed him to work on a variety of projects with an equally varied group of collaborators in fields such as surgery, radiology, biology, and forensics. These projects have resulted in several publications and numerous national and international conference presentations. His research allowed him to combine his varied interests in engineering, art, computer modeling and mathematics.